

1987

Experimental and analytical investigation of the indentation of tubular members /

Joseph A. Padula
Lehigh University

Follow this and additional works at: <https://preserve.lehigh.edu/etd>



Part of the [Civil Engineering Commons](#)

Recommended Citation

Padula, Joseph A., "Experimental and analytical investigation of the indentation of tubular members /" (1987). *Theses and Dissertations*. 4821.

<https://preserve.lehigh.edu/etd/4821>

This Thesis is brought to you for free and open access by Lehigh Preserve. It has been accepted for inclusion in Theses and Dissertations by an authorized administrator of Lehigh Preserve. For more information, please contact preserve@lehigh.edu.

Experimental and Analytical Investigation
of the
Indentation of Tubular Members

by

Joseph A. Padula

A Thesis

Presented to the Graduate Committee

of Lehigh University

in Candidacy for the Degree of

Master of Science

in

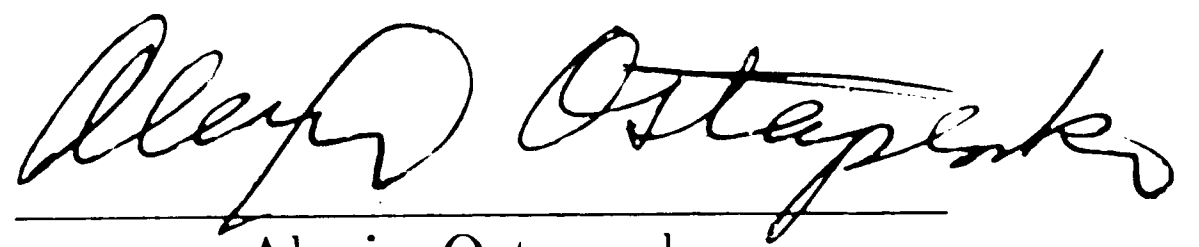
Civil Engineering

Lehigh University

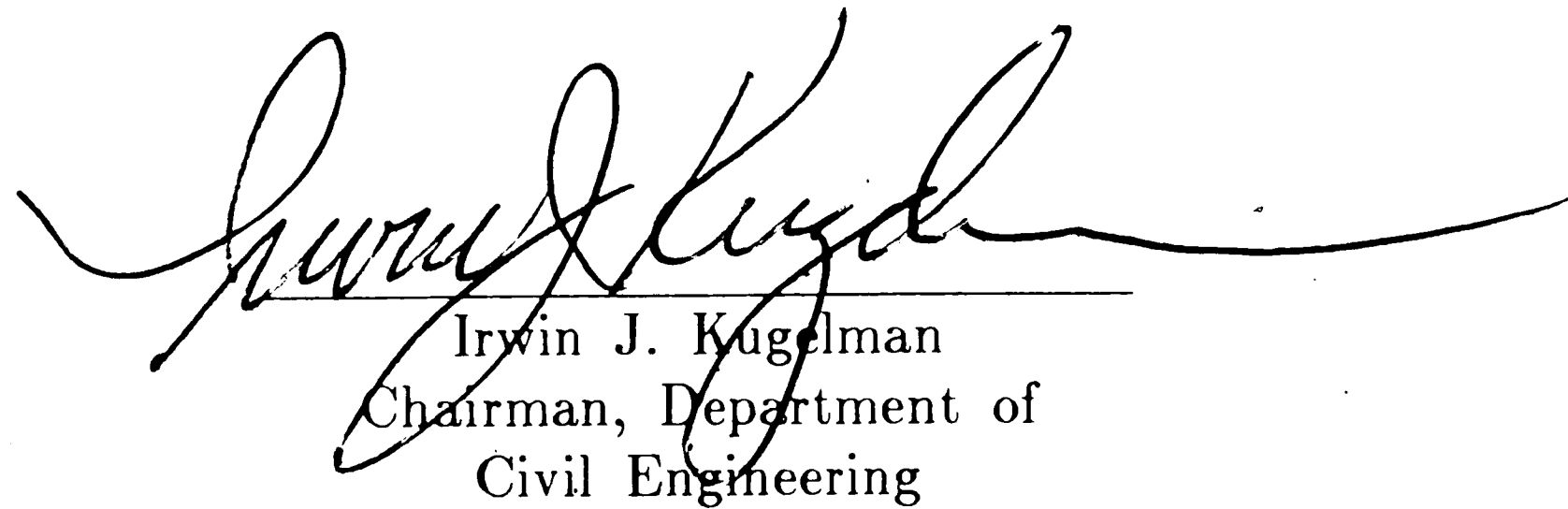
1987

This thesis is accepted and approved in partial fulfillment of the requirements for the degree of Master of Science.

September 23, 1987
(date)



Alexis Ostapenko
Professor in Charge



Irwin J. Kugelman
Chairman, Department of
Civil Engineering

Acknowledgments

This thesis is the product of research conducted at Fritz Engineering Laboratory, within the Department of Civil Engineering at Lehigh University in Bethlehem, Pennsylvania. Dr. Irwin J. Kugelman is the Chairman of the Department of Civil Engineering. The research was part of a project, Residual Strength of Offshore Structures after Damage, which was sponsored by the Minerals Management Service of the U.S. Department of the Interior and the American Iron and Steel Institute under the DOI/AISI Cooperative Research Program. The author is grateful for this support and for the advice and guidance given by the members of the project Task Force; C.E. Smith and A.C. Kuentz, the respective representatives of the sponsoring institutions, and R.H. Wildt (Chairman of the Task Force) of Bethlehem Steel Corporation, C. Capanoglu of Earl and Wright, C.D. Miller of CBI Industries, Inc., J. de Oliveira of Conoco, Inc., and J.B. Gregory of the Minerals Management Service of the U.S. Department of the Interior.

An expression of gratitude is extended to Dr. Alexis Ostapenko for his untiring effort in supervising the research and for his encouragement and guidance in the author's academic endeavor.

Thanks are due to the technical staff of Fritz Engineering Laboratory, especially to Charles F. Hittinger, Robert R. Dales, and Russell C. Longenbach for their help in conducting the experimental work and to Richard N. Sopko for the photographic work. The assistance of Jyh-Min Liaw in conducting the tests is also appreciated.

Special thanks are also due to members of the Lehigh University Computing Center staff, in particular, Stephen O. Lidie and Sandra L. Johnson

for their assistance with the computational work and patience in tutoring the author in the use of a new operating system. The efforts of Dean Krause in keeping the hardware on line under the strain of the analysis are appreciated. The author is also grateful to Monica A. Newman who made special efforts to facilitate his work.

Lastly, the author wishes to express his sincerest gratitude to E. Hunnisett and E.L. Edwards for their support and encouragement over the last years.

Table of Contents

Abstract	1
1. Introduction	2
1.1 Scope	3
1.2 Previous Work	3
1.3 Present Investigation	5
1.3.1 Experimental Work	5
1.3.2 Analytical Work	6
2. Experimental Work	7
2.1 Description of Test Specimens	7
2.1.1 Fabrication and Modification of Test Specimens	7
2.1.2 Dimensions and Material Properties	8
2.2 Indentation of the Test Specimens	8
2.2.1 General Considerations	9
2.2.2 Arrangement and Procedure for Indentation of Specimens	9
2.2.3 Results of Indentation	12
2.2.3.1 Dent Geometry	12
2.2.3.2 Energy Dissipation	12
3. Finite Element Analysis	13
3.1 Introduction	13
3.2 Modeling	14
3.2.1 Contact Problem	15
3.2.2 Discretization of the Tube	17
3.3 Boundary Conditions	19
3.4 Computational Parameters	20
3.4.1 Formulation of Equations	20
3.4.2 Solution of Equations	22
3.4.3 Development of Analytical Procedure	22
3.5 Results of Analysis	24
3.6 Discussion	24
3.7 Computational Cost	25
4. Effect of Residual Stresses	27
4.1 Residual Stresses in a Circular Ring	27
4.2 Effect of Residual Stresses in a Circular Ring	29
4.3 Limited Range of Effect	30
4.3.1 Plastification and Residual Stresses Due to Indentation	30
4.3.2 Assumed and Observed Deformations	32
5. Summary, Conclusions and Recommendations	34
5.1 Introduction and Scope	34
5.2 Experimental Work	34
5.3 Analytical Work	35
5.4 Conclusions	35
5.5 Recommendations for Future Work	37

Tables	38
Figures	41
References	65
Appendix A. Experimental Work by Others	67
A.1 Scope	67
A.2 Description of Test Specimens	67
A.3 Indentation of Specimens	68
Appendix B. Nomenclature	69
Vita	70

List of Figures

Figure 1:	Set-up for Indentation of Specimen P1	42
Figure 2:	Indentation of Specimen P2	42
Figure 3:	Schematic Representation of Ideal Dent Geometry	43
Figure 4:	Schematic Representation of Test Set-up for Indentation	44
Figure 5:	Experimental Load vs. Dent Depth Curve for Specimen P1	45
Figure 6:	Experimental Load vs. Dent Depth Curve for Specimen P2	46
Figure 7:	Energy Absorption vs. Dent Depth for Specimens P1 and P2	47
Figure 8:	Finite Element Model for Tube Indentation	48
Figure 9:	Typical Stress-Strain Relationship for Stiffening Truss Element	49
Figure 10:	Geometry to Determine ϵ_s	49
Figure 11:	Dimensions for Discretization of Model 2	50
Figure 12:	Dimensions for Discretization of Model 4	51
Figure 13:	Dimensions for Discretization of Model 8	52
Figure 14:	Discretization of Tube - Model 2	53
Figure 15:	Discretization of Tube - Model 4	54
Figure 16:	Discretization of Tube - Model 8	55
Figure 17:	Load vs. Dent Depth, Specimen P1 - Model 2	56
Figure 18:	Load vs. Dent Depth, Specimen P1 - Model 4	57
Figure 19:	Load vs. Dent Depth, Specimen P2 - Model 4	58
Figure 20:	Load vs. Dent Depth, Specimen IIII - Model 4	59
Figure 21:	Load vs. Dent Depth, Specimen IBII - Model 8	60
Figure 22:	Load vs. Dent Depth, Specimen IIAII - Model 8	61
Figure 23:	Residual Stresses Through Thickness Due to Cold-Rolling	62
Figure 24:	Stress Distribution after Flattening	62
Figure 25:	Assumed Deformation of a Ring (From Reference [15])	63
Figure 26:	Deformation of a Ring from Idealized Dent Geometry	63
Figure 27:	Test Setup for Indentation (From Reference [12])	64

List of Tables

Table 1:	Specimen Data	39
Table 2:	Computational Cost	39
Table 3:	Details of Analytical Models	40

Abstract

The "damage design" approach to offshore structure design requires consideration of accidental damage and its effect on the structural integrity. For this reason, an experimental and analytical investigation of the indentation behavior of tubular members was conducted.

The experimental work consisted of the indentation of two large-diameter fabricated steel specimens. The test specimens were 1.0 m (40 in.) and 1.5 m (60 in.) in diameter with corresponding D/t ratios of 151 and 227. Each specimen was simply supported at its ends and subjected to a concentrated lateral loading with a rigid indenter at midlength. Load-deformation response and the energy absorption as functions of dent depth are presented for each specimen.

The analytical work included the finite element analysis of the indentation of the two test specimens and of three additional specimens whose indentation response was reported in the literature. In contrast to the two fabricated test specimens, these specimens were manufactured stress relieved tubes. The correlation of the load vs. dent depth response of these tubes with the analytical results was much better than that of the fabricated specimens. This observation prompted an investigation into the effect of residual stresses (due to cold-rolling during fabrication) on the indentation response.

It was shown that these residual stresses can significantly affect the load-deformation relationship by reducing the amount of energy absorbed for a given dent depth. Consequently, neglecting their effect can result in an underestimation of the damage resulting from a given "design collision".

Chapter 1

Introduction

In the design of offshore platforms, it is necessary to consider the possibility of structural damage resulting from accidental impacts during construction or operation, a ship/platform collision, ice hazards, or severe cases of overloading. Of these, ship/platform collisions occur fairly frequently and are probably the single most common type of offshore accident resulting in structural damage. [5] Although it may be impractical to design structures to resist a collision with a large vessel such as a tanker while sustaining only moderate damage, the design process must include consideration of the more probable collisions with supply vessels or other ship traffic. Limiting the extent of the accidental damage in such an event so that the integrity of the structure is not significantly compromised or that it can be maintained until repairs can be effected should be an objective of any design. This requires that the designer be able to estimate the extent of damage that may be expected as well as the residual strength of the structure after damage.

Requiring that the structural integrity of a platform be maintained in the event of an accidental collision necessitates that the structure have sufficient capacity to sustain elastic and plastic deformations thereby providing a mechanism for absorption of energy. Even though elastic deformations and/or vibrations may dissipate most of the energy from minor ship/platform collisions or accidental impacts, plastic deformations will develop at least at the point of contact. [5]

1.1 Scope

To determine the effect of damage, it is first necessary to have some, at least approximate, knowledge of the type and extent of damage that can be reasonably expected as a result of a collision. In framed structures constructed of steel tubular members, the result of a collision usually takes the form of localized dents and/or overall deflection of a member(s). The interaction of these two deformation modes is complex and depends upon the geometry of the member, the end restraint interaction by the frame, and the type of event producing the damage. From knowledge of the member/structure response the energy absorption capacity can be determined providing a means to estimate the extent of damage given a "design collision" with a known mass and velocity.

Therefore, determination of the load deformation response and energy absorption capacity of a structure is prerequisite to prudent design. For these reasons, the current research has been focused on the determination of the indentation behavior of tubular steel members.

1.2 Previous Work

A number of researchers have investigated the indentation of tubular members as it relates to accidental damage in offshore structures. [12, 11, 10, 14, 15] Lateral loading of tubular members and the resulting deformation mechanisms have been the focus of much of the research effort. The approaches to the problem range from simplified analytical models and the use of numerical techniques such as the finite element method to the formation of an experimental database. For example, the basis for Taby's work on the residual strength of damaged tubular members has involved extensive experimental work including the indentation of tubular members. [13] On the

other hand, Wierzbicki and Suh have presented a purely theoretical analysis of the denting of tubular members under combined bending and axial loading. [15] Their work involved the application of a method previously applied to the axisymmetric buckling of tubes. [16] Soares and Soreide have presented a simplified analysis of tubular members whose primary mode of deformation is overall beam deflection and correlated the results with finite element analyses. [11] An excellent review of the state of the art of the collision-damage and residual strength of offshore structures including a comprehensive bibliography has been provided by Ellinas. [5]

Since they are usually based on simplifying idealizations, the proposed analytical solutions must be validated by correlation with experimental results before they can be used with confidence. These idealizations may range from the common assumption of rigid-plastic material behavior to a prescribed deformation geometry for tubes subjected to lateral loading. Due to the complex interaction of localized denting and overall bending deformations and the wide range of tube geometries and loadings, such assumptions may affect the accuracy of the analytical model.

The need for correlation of theoretical results with experimental evidence also applies to results obtained from numerical techniques such as the finite element method. Additionally, the task of generating solutions for such a complex problem involving material and geometric nonlinearities requires considerable expense in terms of time and computer resources.

Probably the most significant shortcoming of the reported experimental work so far is the lack of data on tubular members fabricated by cold-rolling and welding, which is the usual method of fabrication for offshore structures,

and consideration of members with large D/t ratios. The work described here addresses these needs, at least in part.

1.3 Present Investigation

The thrust of the current research effort has been to determine the response of tubular members under lateral loading assuming the primary mode of deformation to be localized denting of the tube wall. This investigation consisted of experimental and analytical phases. The results of the analytical work were correlated with the experimental work of the current project as well as with the experimental results reported by Taby and Rashed in Reference [12]. A brief description of the experimental work performed by Taby and Rashed is given in Appendix A.

1.3.1 Experimental Work

The experimental phase of the project involved the testing of two large-diameter, fabricated tubular test specimens. Each specimen was subjected to a lateral load at midlength to produce a localized indentation. The specimens were simply supported at the ends during indentation and the load was applied through a rigid indenter. The displacements at several locations were measured and recorded thus providing the necessary data to establish the load vs. dent-depth and the energy dissipation relationships. The experimental work was also a prelude to further experimentation (axial load testing) on the residual strength of damaged tubular members. [9]

1.3.2 Analytical Work

The analytical work consisted of the finite element analysis of the indentation of tubular members and correlation of the results with experimental data. In order to assess the validity of the finite element analysis over a wide range of tube geometries and material properties, the analysis and correlation were made for five specimens for which experimental data were available; two specimens tested as a part of this program and three additional specimens for which load vs. dent depth curves were presented in Reference [12]. Correlation with experimental data also provided useful information for refinement of the modeling technique.

The effect of residual stresses due to cold-rolling during the fabrication process on the load vs. dent depth response was also investigated. This was prompted by a much improved correlation between the results of the finite element analysis and the experimental data from the manufactured and stress relieved test specimens reported in Reference [12] as compared to the correlation with data from the fabricated specimens of the experimental phase of this work. The investigation demonstrated that residual stresses can have a significant effect on the indentation response. Specifically, the residual stresses reduce the stiffness of the response and neglecting their effect can result in an underestimation of the damage resulting from a given "design collision".

Chapter 2

Experimental Work

The experimental work consisted of the indentation of two large-diameter, fabricated specimens. The load vs. dent depth response of each specimen was recorded during indentation. Energy absorption as a function of dent depth was also calculated.

Additional experimental data consisting of the indentation response of three specimens (Specimens IIII, IBII, and IIAII) were taken from Reference [12] for correlation with the analytical work. A brief description of this experimental work is given in Appendix A.

2.1 Description of Test Specimens

The specimens were obtained by modifying two test specimens of a previous project (Specimens T3 and T4 in References [8, 6]). For the current project, these two specimens were designated P1 and P2, respectively.

2.1.1 Fabrication and Modification of Test Specimens

The two test specimens, P1 and P2, were fabricated by cold-rolling steel plate into right circular cylinders in a pyramid three-roller bending machine and welding the longitudinal seam by an automatic submerged-arc process. Steel end rings were welded to each end of the specimens to facilitate uniform distribution of the axial load during testing. Detailed information on the fabrication and material properties is given in Reference [8].

Previous axial load testing resulted in severe local buckles confined to one end of each specimen. The limited extent of the deformations made it possible to modify these specimens for reuse by removing the buckled portions and

reattaching the end rings. The modification process is further described in Reference [9].

2.1.2 Dimensions and Material Properties

Specimens P1 and P2 had outside diameters of 1.02 m (40.2 in.) and 1.53 m (60 in.), respectively. Both specimens had a wall thickness of 6.73 mm (0.265 in.). After modification, Specimen P1 was 2.44 m (96 in.) in length and Specimen P2 2.13 m (84 in.), exclusive of the thickness of the end rings. The circular steel end rings welded to the ends of the specimens were 22 mm thick by 127 mm wide (7/8 in. x 5 in.). All pertinent geometric and material properties including diameter-to-thickness (D/t), length-to-radius of gyration (L/r) and dent depth-to-diameter (d/D) ratios are listed in Table 1.

The specimens were fabricated from ASTM A36 steel plate. In the previous project the static and dynamic yield stresses of the material were determined from standard ASTM coupons. [8] The material properties of the modified specimens were assumed to be the same as those of the original specimens. Thus, the possible effects of cold-rolling and work hardening during the original tests were neglected.

2.2 Indentation of the Test Specimens

The indentation of the specimens was accomplished by the application of a lateral load through a rigid indenter. The load vs. dent depth relationship and energy absorption as a function of the dent depth were determined for each specimen from the data collected during indentation.

2.2.1 General Considerations

Although damage to a tubular member due to impact may result in localized dents, overall deflection or a combination of both, the experimental phase of this project dealt only with localized denting. Consequently, the indentation of the specimens was undertaken with the goal of producing dents with little overall distortion of the member.

Consideration was given to various dent geometries, e.g., vee (resulting from a "knife edge" loading), rounded or flat. The selected shape was a localized flattening of the cylinder surface as shown in Fig. 3. The flat portion of the dent measured longitudinally along the specimen was 175 mm (7 in.) in width. The length of the dent (measured transversely across the specimen) was largely controlled by the depth and was approximately equal to the chord distance subtended by a circular arc with a middle ordinate equal to the dent depth.

The dent was located at mid-length of each specimen. The longitudinal centerline of the dent was offset by 120° of arc from the longitudinal weld seam. (The actual location for Specimen P1 was approximately 38 mm (1.5 in.) closer to the weld seam.)

2.2.2 Arrangement and Procedure for Indentation of Specimens

The arrangement for indentation was designed to introduce a dent, as well as, to obtain data on the energy dissipation characteristics of the test specimens. The same set-up was used for both specimens; it consisted of a reaction frame, a load transmission assembly and instrumentation.

The set-up was made in a universal testing machine which served as the reaction frame. As shown in Fig. 1, the test specimen was placed horizontally

on the floor of the testing machine and supported by steel blocks under the end rings. The blocks, in effect, provided simple support at the ends of the specimen and also gave the necessary clearance to place dial gages underneath the specimen.

The load transmission assembly between the machine head and the specimen consisted of a short section of wide flange beam placed transversely across the specimen, a manually operated hydraulic jack, and a load cell. The 175 mm (7 in.) wide flange of the beam served as the die for forming the dent. A view of the indentation of Specimen P2 in progress is shown in Fig. 2. The test setup is shown schematically in Fig. 4. Internal bracing with struts and transverse bearing members was installed at the edges of the intended indentation in order to localize the deformation.

The instrumentation for measuring the distortion of the specimens during indentation consisted of ten mechanical dial gages located as shown in Fig. 4. Two were placed between the beam and the testing machine head, one on each side of the jack-load cell assembly. These gages directly measured the extension of the jack and, thus, the displacement relative to the machine head. Four dial gages were placed between the top surface of the specimen and the testing machine head, and three between the testing machine floor and the bottom of the specimen. One dial gage was used to directly measure the displacement of the machine head relative to the floor. This was done by connecting a dial gage mounted on a pedestal on the floor with a light-gage wire to a magnetic clip on the testing machine head.

The indentation procedure consisted of incremental application of load to the specimen through the jack-loadcell-beam assembly. At each load increment,

the load and dial gage readings were recorded. The approximate depth of dent was indicated by the readings from the dial gages between the machine head and the beam. Loading continued until the dent exceeded the desired depth by an amount estimated to be lost due to elastic recovery during unloading. The set-up and procedure for indentation were similar for both specimens.

Specimen P1 required two cycles of loading and unloading because the elastic recovery was underestimated in the first cycle. The observed elastic recovery during the first unloading provided a means of more accurately estimating the final dent depth. The maximum load needed for P1 was 168 kN (37.8 kips).

During loading of Specimen P2, at approximately 160 kN (36 kips), one of the wooden struts used for internal bracing failed suddenly, and the load immediately dropped to 116 kN (26 kips). The specimen was then unloaded, and the wooden struts were replaced with steel members. Loading then continued to 276 kN (62 kips).

Plots of the load vs. dent depth for each specimen are shown in Figs. 5 and 6. The load was non-dimensionalized with respect to a factor $\left(\frac{4D^2t\sigma_y}{L}\right)$, the magnitude of a concentrated load at midspan which would produce a plastic moment according to simple beam theory. The dent depth is given as a fraction of the tube diameter.

2.2.3 Results of Indentation

The indentation tests produced two specimens with localized dents at midlength as well as data on the load vs. dent depth response. The energy dissipation as a function of dent depth was also determined.

2.2.3.1 Dent Geometry

Locally, the depth of dent for Specimen P1 was 19 mm (0.75 in.), the depth being measured with respect to the points just outside the dented area. Subsequent measurements of the specimen geometry with respect to the ends of the specimen showed that the overall depth of indentation was 28 mm (1.1 in.). This indicated that the deformation was a combination of a local dent and an overall deflection of the specimen wall. For Specimen P2, the depth of dent was 70 mm (2.8 in.) locally and 84 mm (3.3 in.) overall.

Thus, the nature of the dent was also predominantly local with only a slight overall distortion of the specimen. The dentdepth-to-diameter ratios for Specimens P1 and P2 were 2.7% and 5.5%, respectively.

The surfaces of the dented specimens were mapped and contour plots were made. A complete description of the dent geometry of both specimens including the surface contour plots is given in Reference [9].

2.2.3.2 Energy Dissipation

The amount of energy dissipated during the indentation process was determined from the area under the curve plotted from the load vs. dent depth data. Figure 7 shows the total energy absorbed vs. the dent depth for each specimen. The total energy absorbed included both the elastic and plastic deformations since this would be of interest in considering the mechanics of a collision.

Chapter 3

Finite Element Analysis

In order to investigate the tube indentation problem analytically, finite element models were developed and solutions were obtained using the 1981 version of the program ADINA.* This program was selected for its capability regarding material and geometric nonlinearities. The analysis was performed on a Control Data Corporation Cyber 180 Model 850 computer running the NOS and NOS/VE operating systems.

The indentations of Specimens P1 and P2 as well as Specimens IBII, IIAII, IIIII were analyzed with ADINA. Pertinent information on the latter three specimens which are a representative sampling of the specimens tested by Taby and Rashed are given in Appendix A and Reference [12]. These five specimens covered a wide range of tube geometries and material properties for which results of the analysis could be compared to experimental data. The basic modeling technique used is similar to that employed by Hypponen and Raiko in the analysis of a pipe whipping against a rigid support. [7]

3.1 Introduction

The response of a tubular member subjected to indentation is highly nonlinear due to the large deformations of the tube and plastification of the material. The analysis is also complicated by the nature of the contact between the indenter and the tube wall. The contact area increases with the dent depth and the distribution of the load over the contact surface is continuously

*ADINA Engineering AB, Vasteras, Sweden, and ADINA Engineering Inc., Watertown, Massachusetts

changing. Because the contact area and the distribution of the load are both dependent on the response of the tube, the applied load (actually, an induced nodal point displacement) could not be given as prescribed input for the computer program. This necessitated the use of a special modeling technique. The material and geometric nonlinearities due to plastification and large deformations were within the capabilities of ADINA, and the difficulty was only in determining computational parameters such as load increments and response tolerances.

3.2 Modeling

The finite element model consisted of two basic components: an assemblage of shell elements representing the tube and a set of truss elements designed to model the contact between a rigid indenter and the tube wall. The shell elements used the isoparametric shell elements with variable number of nodes from the ADINA element library. Two node truss elements with nonlinear stress-strain relationships were used to model the rigid indenter. The internal bracing used during the indentation of Specimens P1 and P2 was modeled with a single linear elastic truss element. Due to symmetry of the problem, only one fourth of the tube was modeled. The tube was sectioned along the longitudinal and transverse planes of symmetry which passed through the center of the indentation. An overall view of a typical model is shown in Fig. 8.

3.2.1 Contact Problem

The problem of modeling the contact of a rigid indenter against a cylindrical tube was simulated by a series of truss elements with nonlinear material properties. At one end, the truss elements were connected to the shell element nodal points in the indentation area of the tube wall. The opposite ends of all the truss elements were connected to a common node at sufficient distance from the surface of the tube to consider the line of action of the forces to be parallel. A prescribed displacement was imposed on this node to produce the indentation of the tube.

The truss elements used to model the indentation of Specimens P1 and P2 were arranged in three rows corresponding to the 175 mm (7 in.) width of the indenter used. Since the specimens tested by Taby were subjected to a knife edge loading, the indentation was modeled with a single row of truss elements on the centerline of the indentation.

Simulation of the contact was achieved through the definition of the constitutive relationships for the truss elements. Nonlinear elastic material property defined by a piecewise-linear stress-strain (σ - ϵ) relationship was selected from the material models available for truss elements in ADINA. Pairs of σ - ϵ values input into the program defined the stress and tangent modulus as functions of strain.

A typical stress-strain diagram for a truss element is shown in Fig. 9. To model the condition of contact (no tension forces may develop between the tube surface and the indenter), the truss elements were made extremely soft in tension by defining a very small modulus of elasticity for positive strains. Modeling of the initial gap between the indenter and the tube was accomplished

by extending the soft material response into the compression range. At the point of contact between the indenter and tube wall the modulus of elasticity was very large. Typically, this range was preceded by a short transition of moderate stiffness (See Fig. 9.).

The values of ϵ_s , the strain at which the modulus of elasticity increases to its ultimate value, were determined for each truss element from the geometry as shown in Fig. 10, where $\epsilon_s = \frac{\delta}{L}$. The transition from an essentially zero modulus of elasticity to rigid was also determined from the geometry. The value of ϵ_s calculated for a truss element marked the initiation of the transitional stiffness for the adjacent truss element. This constitutive relationship allowed the truss elements to have virtually no stiffness until the deformed geometry of the model was consistent with contact at a nodal point by a rigid indenter.

The use of a transition in the stress-strain relationships proved to be computationally expedient. It was also justified in the simulation of the physical problem. In a direct comparison of analyses with bilinear and trilinear stress-strain curves (with and without a transition), the bilinear relationship was slightly more costly, requiring 4% more CPU time for a 13% increase in the number of equilibrium iterations performed for the analysis. The greatest difference in the two runs was in the calculated load vs. dent depth response of the model. The response using a trilinear stress-strain relationship was considerably smoother.

The physical justification for using the transition in moduli of elasticity lies in the continuous nature of the actual distributed loading as opposed to the application of the load at discrete nodal points. The transition simulates a continuous loading by allowing a more gradual shifting of load from one nodal

point to the adjacent node as the dent depth is increased. For this reason, a quad-linear stress-strain relationship (2 transitions) was used in the analyses performed with Model 2 (See Sec. 3.4.3).

3.2.2 Discretization of the Tube

Excluding preliminary attempts, three discretizations of the tube were used. One model was used for the analysis of the test specimens P1 and P2 only, while two other more refined models were used in the analysis of all five specimens. The latter two models differed from the first by the type of shell elements and by the coarseness of the mesh at the indentation. The principal difference between the two latter discretizations was basically a modification to accommodate larger dent depths.

In modeling, advantage was taken of the symmetry of the problem allowing the analysis to be performed on a model consisting of one-fourth of the actual tube. Planes of symmetry, passed through the center of the indentation transversely to and along the longitudinal axis of the tube, divided it into quarter segments. Appropriate boundary conditions were imposed at the cuts (See Sec. 3.3).

A description of the three models is given in the following paragraphs indicating the types of shell elements used and the number of nodal points. In the course of the work, these models were somewhat arbitrarily given the designations Model 2, 4, and 8 corresponding to a scheme for labeling each of the computer runs made. Dimensions related to the discretization for each model and the particular specimens are shown in unfolded views of the meshes in Figs. 11, 12 and 13.

Model 2, the model first used for the analysis of Specimens P1 and P2,

consisted of 32 shell elements and 150 nodal points as shown in Fig. 14. Nine-node shell elements were employed, except for the two elements used as a transition to a finer mesh at the indentation. At the indentation, the circumferential discretization consisted of two elements spanning 20° of arc. Thus, three rows of five nodal points in the circumferential direction were connected to truss elements. The remaining 160° of arc consisted of two elements of 20° and three elements of 40° .

The discretization of Model 4 shown in Fig. 15 consisted of 26 shell elements which, except for the transition elements, were 16-node elements. Thus, this model had a total of 196 nodal points. Due to the much finer mesh in the region of indentation the response produced by this model was much smoother than Model 2. The circumferential discretization at the indentation consisted of six elements spanning 5° of arc each followed by one element with 30° and two elements with 60° . The effect of the finer mesh was an improved simulation of the continuous application of a load distributed over the surface of the tube because of the denser population of truss elements transmitting load to the shell as well as an increased sensitivity to deformations. The use of 16-node shell elements also permitted a more rapid transition from the fine mesh over the indentation to a coarser mesh away from the dented area.

The third discretization, Model 8, was used to accommodate larger relative dent depths. This model, shown in Fig. 16, is a modification of Model 4 with the fine mesh in the region of indentation extending over 60° of arc as opposed to 30° . The mesh in this region was slightly coarser since only six elements in the circumferential direction were used over 60° of arc. This model consisted of 28 shell elements, typically, 16-node, and a total of 227 nodal points.

3.3 Boundary Conditions

The boundary conditions imposed on the models were dictated by two criteria; the enforcement of deformations consistent with the symmetry of the problem and the imposition of the support conditions of the two different test arrangements used for the indentation of Specimens P1 and P2 (See Sec. 2.2) vs. Specimens IIIC1, IBII, and IIAII (See Appendix A).

The boundary conditions required to impose the condition of symmetry on the quarter section model were the same for all five specimens. At the circumferential cut made by the transverse plane of symmetry at the center of indentation, the translational degree of freedom in the longitudinal direction and rotation about a tangent to the circumference were eliminated. Along the two longitudinal cuts made by the longitudinal plane of symmetry, the translation in the circumferential direction, as well as, the rotation about the longitudinal axis were prohibited.

The support condition of the test setup for Specimens P1 and P2 were modeled by preventing translation in the transverse plane at the end of the model. This accommodated the effect of the support arrangement as well as of the end rings attached to these two specimens (See Chap. 2).

The support arrangements for the indentation and the length of the Specimens IIIC1, IBII, and IIAII (See Appendix A), permitted the analytical models to be shortened for the sake of economy of computation. The length of the models was made not less than one and a half diameters since the portions of the tube outside this region would have negligible effect on the indentation. The actual lengths of the models used for these three specimens are given in Figs. 12 and 13. All degrees of freedom were allowed at the truncated free end

of the model. The cradle support for these specimens was modeled by prohibiting translation in the radial direction at the nodal points directly opposite the indentation.

3.4 Computational Parameters

The high degree of nonlinearity of the ~~problem~~ resulting from large displacements coupled with material nonlinearity and the aforementioned contact problem presented some computational difficulties. When unresolved, these difficulties typically manifested themselves in erratic calculated response or abnormal termination of computation. However, results were obtained after gaining some experience with the computer program. In particular, some experimentation was necessary to determine the effect of the various user input parameters which relate to the formulation and solution of the incremental equilibrium equations on the calculated response. In general, the load increments had to be made very small and equilibrium iterations performed at every load step. The stiffness matrix was also updated at every load step. Even with these measures taken, the calculated response was not always as smooth as would be desired.

3.4.1 Formulation of Equations

For the shell elements, total Lagrangian formulation was used (large displacements and rotations with small strains) together with elasto-plastic material behavior. The von Mises yield criterion was used for the material model. [2]

In the formulation of the element matrices, ADINA employs Gauss numerical integration for which the order of integration (number of integration

points) is controlled by the analyst. The program documentation offers somewhat nebulous advice on suggested integration orders but seems to favor higher integration orders for nonlinear analysis. [1, 2] The likely reason is that lower integration orders can result in an assembled structure stiffness matrix that is singular or ill-conditioned. [3] However, it has been suggested that in general "it is best to use as low an order as possible without precipitating a numerical disaster". [4] The first analyses performed with Model 2 used higher integration orders and produced load vs. dent-depth responses that were very much stiffer than the experimental response. The subsequent use of reduced integration orders with this model resulted in a much improved agreement with the experimental data. This may be attributed to the fact that the resulting inaccuracies in the numerical integration may compensate for the inherent stiffness of the finite element solution. [3]

ADINA allows up to 4 integration points in the in-plane directions of the shell elements as well as through the thickness. The default values for the in-plane directions are 2 and 3 for the 9 and 16 node elements, respectively. [1] However, higher integration orders of 3 and 4 respectively are suggested. [2] Although it is suggested that a higher integration order through the thickness may be more effective for elasto-plastic analysis, no significant difference was noted in a comparison of 2 and 3 integration points through the thickness. For the sake of economy of computation, 2 ²point integration through the thickness was used thereafter. Tables 2 and 3 show the integration orders used in the analysis for the various models. A single integration point was used for the truss elements.

3.4.2 Solution of Equations

The Broyden-Fletcher-Goldfarb-Shanno (BFGS) method, which utilizes an updated stiffness matrix for the equilibrium iterations, was selected (as opposed to the modified Newton iteration) to solve the equilibrium equations. Due to its improved convergence characteristics, this is the recommended method when significant nonlinearities are expected. [1, 2] The convergence criteria were the default values in ADINA. Hence, only an energy convergence tolerance was used.

Although some attempts were made at smoothing the calculated response by tightening the convergence tolerances, greater success was obtained by reducing the load increment. This is likely due to the history dependence of the solution because of the elasto-plastic material model used and the local unloading of the shell elements as a result of the redistribution of load over the contact area as the dent depth increased.

3.4.3 Development of Analytical Procedure

The analysis of Specimen P1 was the first to be performed, and the first runs with a reasonable calculated response and correlation with experimental data were achieved with Model 2. The first requisite for an analysis with reasonable correlation to the experimental response with Model 2 was the use of reduced integration orders for the shell elements (2x2 in the in-plane directions since 9 node shell elements were used). This resulted in a significant reduction in the stiffness of the response and provided a much improved agreement with the experimental response as discussed in Sec. 3.4.1.

In order to more closely model the application of a distributed load over the relatively coarse mesh of Model 2 in the region of the indentation,

quad-linear stress-strain relationships for the truss elements were used. That is, two transitions between essentially zero and infinite modulus of elasticity were used causing each truss element to gradually stiffen as the indentation spread circumferentially from one nodal point to the next. However, determination of the specific values of stress and strain at the transitions for each truss element (5 sets) that would result in a reasonably smooth calculated response proved to be a trial and error process requiring considerable effort from the analyst as well as significant computational resources.

Initial attempts at analyzing the indentation of Specimen P2 with Model 2 were abandoned as it was realized that the same trial and error process would have to be repeated. This prompted the development of Model 4 with a much finer mesh in the dented area allowing the use of a single transition in the stress-strain relationships for the truss elements which could be predetermined from the geometry of the model (See Sec. 3.2.1).

The analysis of Specimen IIII was also performed with Model 4. For this analysis it was found that use of higher integration orders (4x4 in the in-plane directions) gave slightly better agreement with the experimental data. However, the difference in the responses calculated with reduced and higher integration orders was not as significant as with Model 2 due to the finer mesh of Model 4.

Model 8 was used in the analysis of Specimens IBII and IIAII in order to accommodate their larger dent depths. Although this model produced results which correlated well with the experimental response overall, the slightly coarser mesh of Model 8 is reflected in the lack of smoothness of the calculated response.

3.5 Results of Analysis

The analytical results are presented as comparisons of the calculated and experimental load vs. dent depth responses. In each case, the response is shown in non-dimensionalized form, the load being expressed as a fraction of the magnitude of a concentrated load at midspan which would produce a plastic moment according to simple beam theory, and the dent depth is given as a percentage of the diameter. All pertinent information related to the computation, such as the specimen analyzed, number of load increments, integration order for the shell elements, and the model used is given in Table 3.

The load vs. dent depth response for Specimen P1 calculated with Model 2 is shown in Fig. 17 along with the experimental response. The results of the analysis of Specimens P1 and P2 with Model 4 and their experimental response are shown in Figs. 19 and 18. The analytical and experimental response of Specimen IIII is shown in Fig. 20. Figures 21 and 22 show the responses of Specimens IBII and IIAII from the analysis with Model 8.

3.6 Discussion

The validity of the finite element analysis was verified by comparison of the calculated response with the experimental. The correlation with the experimental data from the two large-diameter, fabricated specimens was not as good as was obtained for the smaller, manufactured specimens which had been stress relieved. Specifically, the calculated response was initially much stiffer than the experimental for the fabricated specimens as shown in Figs. 17, 18, and 19. An implication is that residual stresses which are not taken into account in the finite element analysis but are present in the fabricated specimens have a softening effect on the indentation response. The residual

stresses due to cold-rolling were assumed to be significant and an investigation of their effect was made. The results are discussed in Chap. 4.

The effect of the number of integration points used in the calculation of the shell element stiffness matrices also seemed to have a significant effect for the responses calculated with Model 2. However, the effect of integration orders on the response calculated with Model 4, which has a much finer mesh, was not nearly as great. This supports the reasoning that the inaccuracy resulting from reduced integration orders may offset the excessive stiffness inherent in a coarse mesh as discussed in Sec. 3.4.1.

3.7 Computational Cost

The computational work was executed on a Control Data Corporation Cyber 180 Model 850 computer running the NOS and NOS/VE operating systems. For the most part, the NOS/VE operating system was used because it was more economical than the NOS operating system. Two benchmark jobs were run to compare costs under the two operating systems. In each case the run under the NOS/VE operating system showed a cost savings in CPU time of better than 40%.

The cost of each analysis in terms of CPU time varied with each of the three models. It was also sharply dependent on the integration order used with the shell elements, but otherwise was generally consistent in terms of CPU time per load step for each model. Computational times listed in Table 2 are representative values for the runs made with each model.

Cost for each run varied considerably. At the high extreme, CPU time per load increment for Model 8 with reduced integration orders averaged 57 seconds and over 300 load increments were used in the analysis of a dent depth

equal to 10% of the diameter. This required several hours of CPU time for a single load-deformation relationship. More typically, 150 to 200 load increments were used with 12 to 36 CPU seconds per increment. The obvious conclusion is that considerable computational resources are required to conduct such a finite element analysis.

Chapter 4

Effect of Residual Stresses

The much improved correlation between the results of the finite element analysis (which does not include consideration of residual stresses) and the experimental data on the manufactured, stress relieved specimens (Specimens IBII, IIAII, and IIICI) in comparison with the fabricated specimens (Specimens P1 and P2) prompted the investigation into the effects of residual stresses on the indentation behavior.

To gain an appreciation of the phenomenon, the formation of a circular ring from a straight bar was analyzed since the residual stresses that develop are analogous to the rolling residual stresses in a fabricated tube. The analogy was extended to the indentation of a tube by considering the flattening of a segment of the ring. The results showed that the residual stresses in a ring had a significant effect on the moment required to flatten a segment of the ring.

4.1 Residual Stresses in a Circular Ring

As a first step in determining the effect of residual stress on the indentation behavior, the magnitude and pattern of residual stresses in a ring resulting from cold-bending were determined. This was readily done considering elastic-perfectly plastic material property and a rectangular cross section. An equation for the initial curvature, Φ_i , required to produce a ring with a final curvature Φ (equal to the reciprocal of the radius, $\frac{1}{R}$) is given by;

$$\left(\frac{\Phi_i}{\Phi_y}\right)^3 - \left(\frac{3}{2} + \frac{t}{D\epsilon_y}\right)\left(\frac{\Phi_i}{\Phi_y}\right)^2 + \frac{1}{2} = 0 \quad \text{for } \Phi \geq \Phi_y \quad (4.1)$$

where

t = the wall thickness

D = the diameter of the ring

ϵ_y = the yield strain of the material

Φ_y = the yield curvature = $\frac{2\epsilon_y}{t}$

An explicit solution for Φ_i is somewhat difficult to obtain. However, it is possible to make a very good approximation considering that the difference between the initial and final curvatures is equal to 1.5 times the yield curvature i.e., $\Phi_i - \frac{1}{R} = 1.5\Phi_y$. This approximation is very good for values of $\frac{\Phi}{\Phi_y} \geq 2.0$ due to the asymptotic nature of the moment-curvature relationship for elastic-perfectly plastic materials. This lower bound for the approximation translates to $\frac{t}{D\epsilon_y} \geq 2.0$, which, for even moderately high strength steels, say $\epsilon_y \approx 0.0025$, is satisfied for $\frac{D}{t}$ ratios up to 200. With this approximation, which is valid for the range of $\frac{D}{t}$ ratios and yield strains typically encountered in offshore structures, Eq. (4.1) simplifies to

$$\frac{\Phi_i}{\Phi_y} = \frac{\Phi}{\Phi_y} + \frac{3}{2} \quad (4.2)$$

or

$$\Phi_i = \frac{1}{R} + \frac{3\epsilon_y}{t} \quad (4.3)$$

which gives the maximum required curvature in terms of the thickness, yield strain, and the final radius, R . Since the final curvature is equal to $\frac{1}{R}$, and the linearly elastic relaxation curvature must be $\frac{3\epsilon_y}{t}$, the residual stress distribution is as shown in Fig. 23. The residual stress at the outer fiber is equal to 1/2

the yield stress and is opposite in direction to the stress due to rolling. The maximum residual stress, $\sigma_y(1 - 3\alpha)$ where $\alpha = \frac{D \epsilon_y}{2t} + 3\epsilon_y$ occurs at a distance of αt from the neutral axis.

It should be noted that these residual stresses are not in self equilibrium (but only slightly so) due to the approximation made for Eq. (4.2) or (4.3).

4.2 Effect of Residual Stresses in a Circular Ring

With the residual stress distribution for the cold-rolling process known, it is possible to determine the moment required to flatten (return to zero curvature) a segment of the ring by superimposing the stress distribution due to the change in curvature onto the residual stresses. The elastic moment required is directly proportional to the change in curvature. The results of this superposition are shown in Fig. 24.

A comparison of the stresses resulting from flattening a segment of a circular ring with and without residual stresses indicates a reduction in the moment in the flattened region when residual stresses are present. The reduction calculated for a ring having the same radius, thickness, and material properties as Specimen P1 was 21.1% and 22.1% for P2.

Although these calculations are only an approximate attempt to quantify the effect of residual stresses due to cold-rolling plate into tubular members, they support the contention that the residual stresses lead to a significant reduction in the load required to produce an indentation and in the energy dissipated in the process.

4.3 Limited Range of Effect

The load vs. dent-depth relationships for the two fabricated specimens, P1 and P2, shown in Figs. 18 and 19 indicate that, in the initial stages of indentation, the response calculated by ADINA is much stiffer than the experimental response. However, the calculated and experimental curves seem to roughly parallel each other for some distance beyond this initial range.

The limited extent of the range for which the calculated response is stiffer than the experimental response is a consequence of the local plastification and unloading that occur during deformation. This plastification and unloading have a mitigating effect on the residual stresses due to cold-rolling since this process results in the formation of its own residual stresses. An assumed deformation model and observed deformations are used to demonstrate that the effect of residual stresses due to cold-rolling is limited to the initial stages of indentation.

4.3.1 Plastification and Residual Stresses Due to Indentation

A simple model of the deformation of a cross section of a tube subjected to indentation is shown in Fig. 26. The indentation results in local plastification followed by unloading as the localized area of plastification or plastic hinge migrates through a given point in the deformation process. As a result, residual stresses are formed in a manner similar to that resulting from cold-rolling during fabrication and have a similar effect. However, it appears from the comparison of the analytical and experimental results that the effect is not realized until some finite deformation occurs.

Wierzbicki and Suh presented an analytical method for analyzing the denting of tubes under combined loading. [15] Their method involves the analysis of a simplified shell model consisting of a series of rings and

longitudinal strips. The deformation assumed for the ring elements is used here to show that the effect of residual stresses due to cold-rolling is mitigated in the deformation process. A deformed ring was assumed to be divided into four segments of constant curvature separated by moving hinges as shown in Fig. 25. Although this deformation is not consistent with indentation due to lateral loading, it does approximate observed deformations.

The shape of the deformed ring for a given dent depth, d , is a function of three parameters, R_1 , R_2 , and θ defined in Fig. 25. From the assumed geometry and the assumption of inextensibility of the ring in the circumferential direction, the following two equations are obtained:

$$R_1\theta + R_2(\pi - \theta) + (R_1 - R_2)\sin\theta = \pi R \quad (4.4)$$

$$d = 2R - \{R_1(1 - \cos\theta) + R_2(1 + \cos\theta)\} \quad (4.5)$$

Since one more equation is needed to define the assumed geometry in terms of the dent depth, the following relationship was suggested:

$$R_2 = \left(\frac{\theta}{\theta_0}\right)^n R \quad (4.6)$$

Wierzbicki and Suh further suggest that $n=1$ and that θ_0 , the initial value of θ (undeformed geometry), be set to $\frac{\pi}{2}$ resulting in the relationship

$$R_2 = \frac{2\theta}{\pi} R \quad (4.7)$$

With this assumed deformation field, the curvature of the segments adjacent to the flattened portion of the ring increases since R_2 decreases with increasing dent depth. Plastification ensues as the change in curvature in these segments increases beyond the yield curvature $\left(\frac{1}{R_2} - \frac{1}{R} > \Phi_y\right)$. As the deformation increases, the hinges adjacent to the flattened segment migrate apart, resulting

in a reversal in curvature from one side of the hinge to the other. If plastification has occurred in the segments with radius R_2 , the moment required for this reversal in curvature is reduced. The condition for incipient plastification is given by

$$r_2 > \frac{t}{D\epsilon_y + t} \quad (4.8)$$

where $r_2 = \frac{R_2}{R}$.

This local plastification followed by a reversal in curvature is analogous to cold-rolling and then flattening (denting). The relative dent depth at which plastification is initiated is determined from Eqs. (4.4), (4.5) and (4.7) and is given by

$$\frac{d}{D} = 1 - \left[\frac{\pi(1-r_2) + r_2(\theta + \sin \theta)}{2(\theta + \sin \theta)} (1 - \cos \theta) + \frac{r_2}{2} (1 + \cos \theta) \right] \quad (4.9)$$

The solution of Eqs. (4.8) and (4.9) for the dent depths at which plastification initiates in Specimens P1 and P2 gives the relative dent depths of 6.1% and 10.3%, respectively. This indicates that the residual stresses due to denting deformation have no effect until a finite dent depth is reached. However, these calculated values of the dent depth are obviously dependent on the assumptions made for the deformed shape.

4.3.2 Assumed and Observed Deformations

The calculated relative dent depth at which the effect of residual stresses is mitigated by plastification during deformation is higher than is indicated by the comparison of the analytical and experimental load vs. dent depth curves (Figs. 18 and 19). This is apparently due to the assumed deformation geometry used in the calculations.

Although Wierzbicki and Suh based their assumed deformation on observation of test specimens and certain analytical considerations, the deformations observed for Specimens P1 and P2 differed somewhat from this assumed geometry. The primary difference was in the formation of yield lines around the flattened section of the tube similar to the idealized dent geometry shown in Fig. 3. The actual deformation of P1 and P2 resemble the geometry shown in Fig. 3 rather than the cross sectional geometry of Wierzbicki and Suh's model shown in Fig. 25. This is likely due to the relatively high D/t ratios of these two specimens. A deformation model of a ring with migrating plastic hinges based on the geometry shown in Section A-A of Fig. 3 is shown in Fig. 26. The two plastic hinges migrate apart as the dent depth and the length of the flattened segment of the ring increase. The effect of the formation of a plastic hinge followed by a reversal in curvature (flattening), as the plastic hinges migrate, is the same as discussed in Sec. 4.3.1.

According to this deformation model, the formation of the migrating plastic hinges occurs at infinitesimal dent depth. This means that the effect of residual stresses due to cold rolling would be immediately nullified. Thus, this model obviously does not reflect the actual deformation process but does provide a qualitative indication that the dent depths calculated in Sec. 4.3.1 should be greater than the actual values. Hence, the dent depth at which the effect of residual stresses becomes insignificant in the deformation process is somewhat less than calculated from Eqs. (4.8) and (4.9), especially for tubes with large D/t ratios.

Chapter 5

Summary, Conclusions and Recommendations

5.1 Introduction and Scope

The investigation of the indentation behavior of tubular members reported here consisted of experimental and analytical phases.

The experimental phase of the project provided data on the indentation behavior and energy dissipation of two large-diameter fabricated tubular specimens. The data together with the results of three tests conducted by others were compared with the results of the analytical work.

The analytical phase of the project consisted of a finite element analysis of the indentation problem. The program ADINA was used because of its capability for performing large displacement materially nonlinear analysis. Some innovative modeling techniques were employed to simulate the contact of a rigid indenter with the tube wall.

5.2 Experimental Work

An indentation was introduced into two large-diameter, fabricated tubular specimens by the application of a lateral load through a rigid indenter. The load vs. deformation response during indentation was used to calculate the energy absorption as a function of the dent depth for each specimen. Both specimens exhibited similar characteristics in this regard.

5.3 Analytical Work

The finite element analysis of the indentation of the test specimens was performed with the ADINA program which has the capability for material and geometric nonlinearities. To further assess the validity of the finite element modeling over a broader range of tube geometries and materials, the analysis was extended to include the indentation of three additional specimens from Reference [12]. In contrast to the two test specimens of the current program, these small-scale specimens were manufactured stress relieved tubes.

The finite element model consisted of an assemblage of shell elements to model the tube and a set of truss elements to simulate the application of a lateral load through a rigid indenter. Due to the high degree of nonlinearity inherent in the problem as a result of large deformations, plastification, and the nature of the loading, the incremental analysis had to be performed with a large number of load steps.

The correlation of the analytical and experimental results was significantly better for the manufactured stress relieved specimens than for the fabricated specimens. This prompted the investigation of the effect of residual stresses due to cold-rolling. The results of the investigation confirmed the discrepancies in the behavior of the fabricated and manufactured specimens.

5.4 Conclusions

The finite element method, specifically, the commercially available general analysis programs, can be used for predicting the elastic-plastic large-deformation response of tubular members subjected to concentrated lateral loads.

However, the finite element analysis of a nonlinear system is not always a well defined or direct process. The modeling of the physical problem may not

be straightforward; it may require innovative techniques or may only be an approximation due to the limitations of the computer program. Both of these situations were encountered in the analytical work in modeling the contact with a rigid indenter. Furthermore, several other factors can affect the results of the analysis. These can be the types of elements used and the discretization of the model to variations in the way the governing equations are formed and solved within the program. To determine the effect of these factors on the results, the analyst may have no alternative other than to perform further analyses with a rediscritized mesh or modified computational parameters. Obviously, this can be an expensive process, in terms of both time and computational resources.

In view of the above considerations and of the results of this investigation, acceptance of the analysis should be contingent on an investigation of the ramifications of the modeling and the assumptions made in the analysis. Ideally, the analyst should have some empirical evidence with which to correlate the solution. Specifically, the results of this investigation indicate that the indentation behavior of full scale fabricated tubular members may vary significantly from the behavior predicted by a finite element analysis. This is due, at least in part, to residual stresses in the fabricated members.

Since it has been shown that residual stresses can have a fairly significant effect on the indentation response, some consideration should also be given to the application of experimental results obtained from stress relieved specimens to the behavior of fabricated structures.

5.5 Recommendations for Future Work

In order to develop a more complete understanding of the indentation behavior of tubulars, research is needed to generate a more complete set of data. Simplified procedures for determining the indentation behavior could then be developed from this database. Experimental work, particularly full scale testing is suggested in conjunction with analytical methods. An effort should also be made to quantify the effects of residual stresses or incorporate them into the analytical methods.

In light of the results of this investigation it is recommended that results, whether obtained through numerical methods, simplified analytical treatment, or experimentation, be correlated with full scale testing. Specifically, more indentation tests are needed on specimens fabricated by cold-rolling and welding and thus having residual stresses which are typical for real structures.

Tables

Table 1: Specimen Data

Spec. No.	F _{ys}	Dimensions					Dent Depth	
		OD	t	L	D/t	L/r	d	d/D
	(MPa)	(m)	(mm)	(m)			(mm)	(%)
P1	203.8	1.02	6.73	2.44	150.7	6.80	28	2.7
P2	203.8	1.53	6.73	2.13	226.5	3.96	85	5.5
IBII	230	0.125	2.51	3.5	49.9	79.1	12.5	10.0
IIAII	351	0.161	2.52	3.5	63.6	61.8	16.1	10.0
IIICI	472	0.250	6.02	3.5	41.6	39.5	12.6	5.0
	(ksi)	(in.)	(in.)	(in.)			(in.)	(%)
P1	29.56	40.2	0.265	96.0	150.7	6.80	1.1	2.7
P2	29.56	60.3	0.265	84.0	226.5	3.96	3.3	5.5
IBII	33.4	4.93	0.099	138	49.9	79.1	0.492	10.0
IIAII	50.9	6.31	0.099	138	63.6	61.8	0.633	10.0
IIICI	68.5	9.86	0.237	138	41.6	39.5	0.496	5.0

Table 2: Computational Cost

Model	Shell Element Integration Order		CPU time/Load Step (sec.)
	In-Plane	Through Thickness	
2	2	3	16
2	2	2	12
2	3	3	27
4	3	2	36
4	4	2	66
8	3	2	57

Table 3: Details of Analytical Models

Specimen	Analytical Model No.	Shell Element Integration Order	Number of Load Increments	Load vs. Dent Depth Response
P1	2	2x2x3	144	Fig. 17
P1	4	3x3x2	144	Fig. 18
P2	4	3x3x2	172	Fig. 19
IIICI	4	4x4x2	172	Fig. 20
IBII	8	3x3x2	332	Fig. 21
IIAII	8	3x3x2	302	Fig. 22

Figures



Figure 1: Set-up for Indentation of Specimen P1

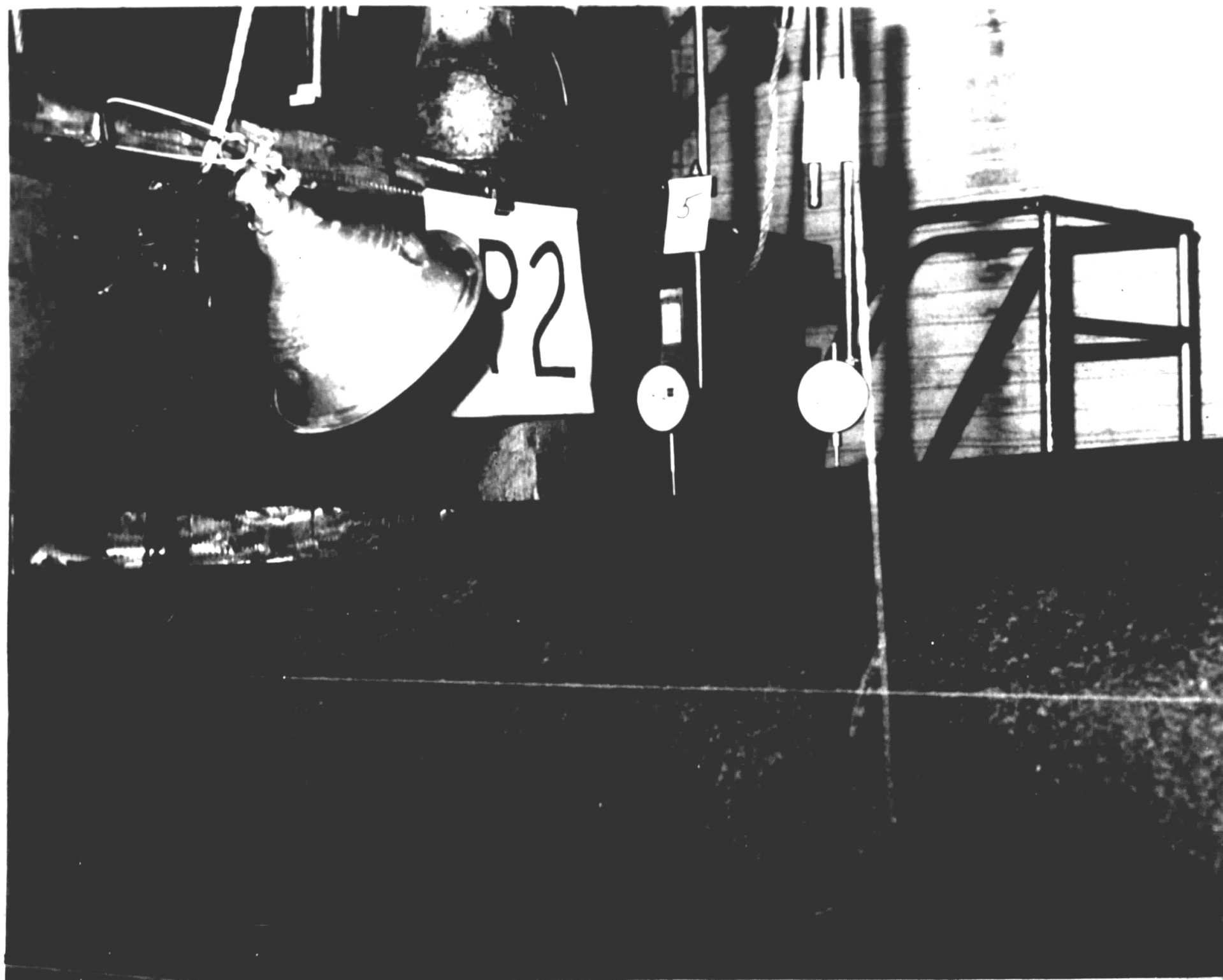


Figure 2: Indentation of Specimen P2

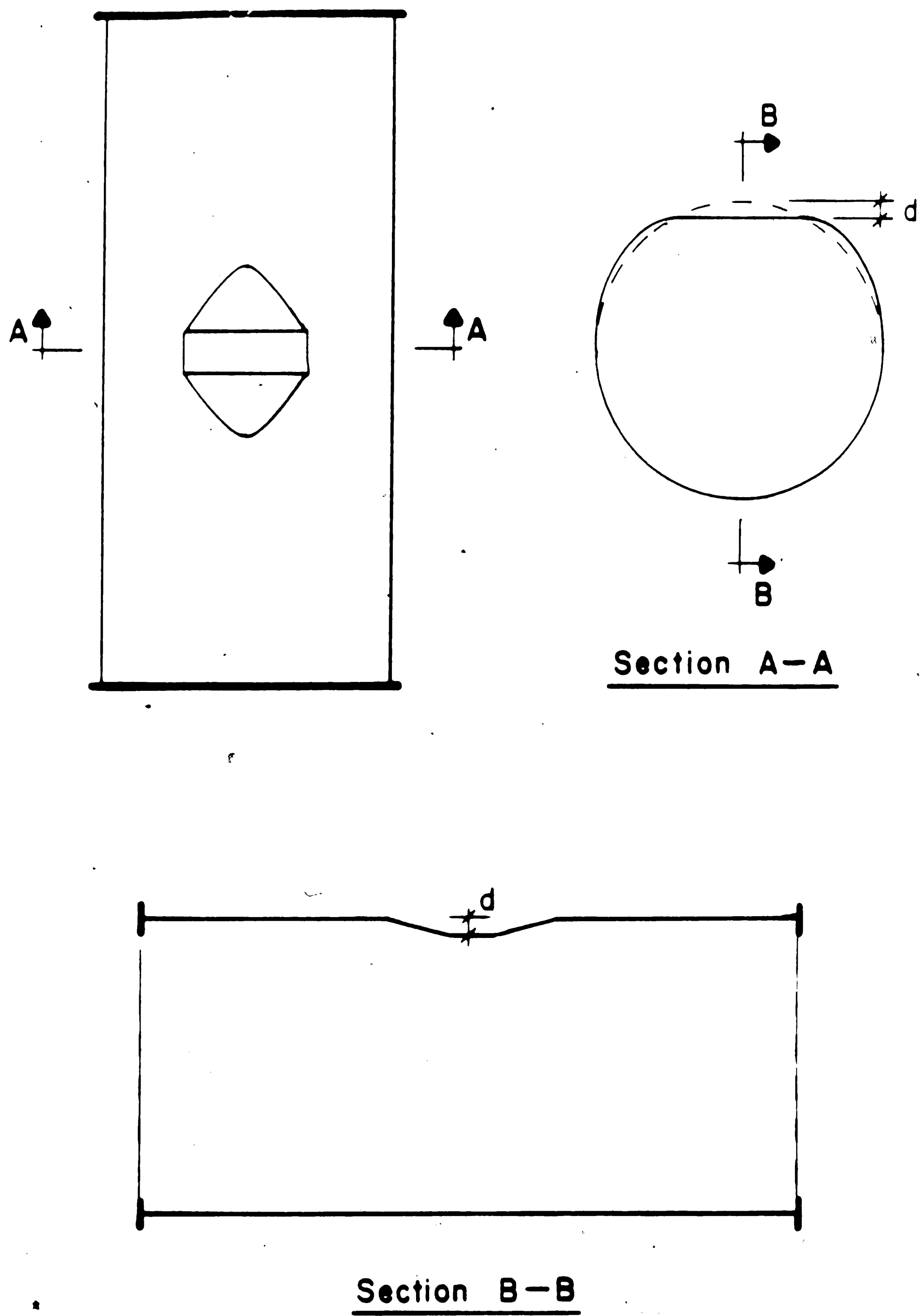
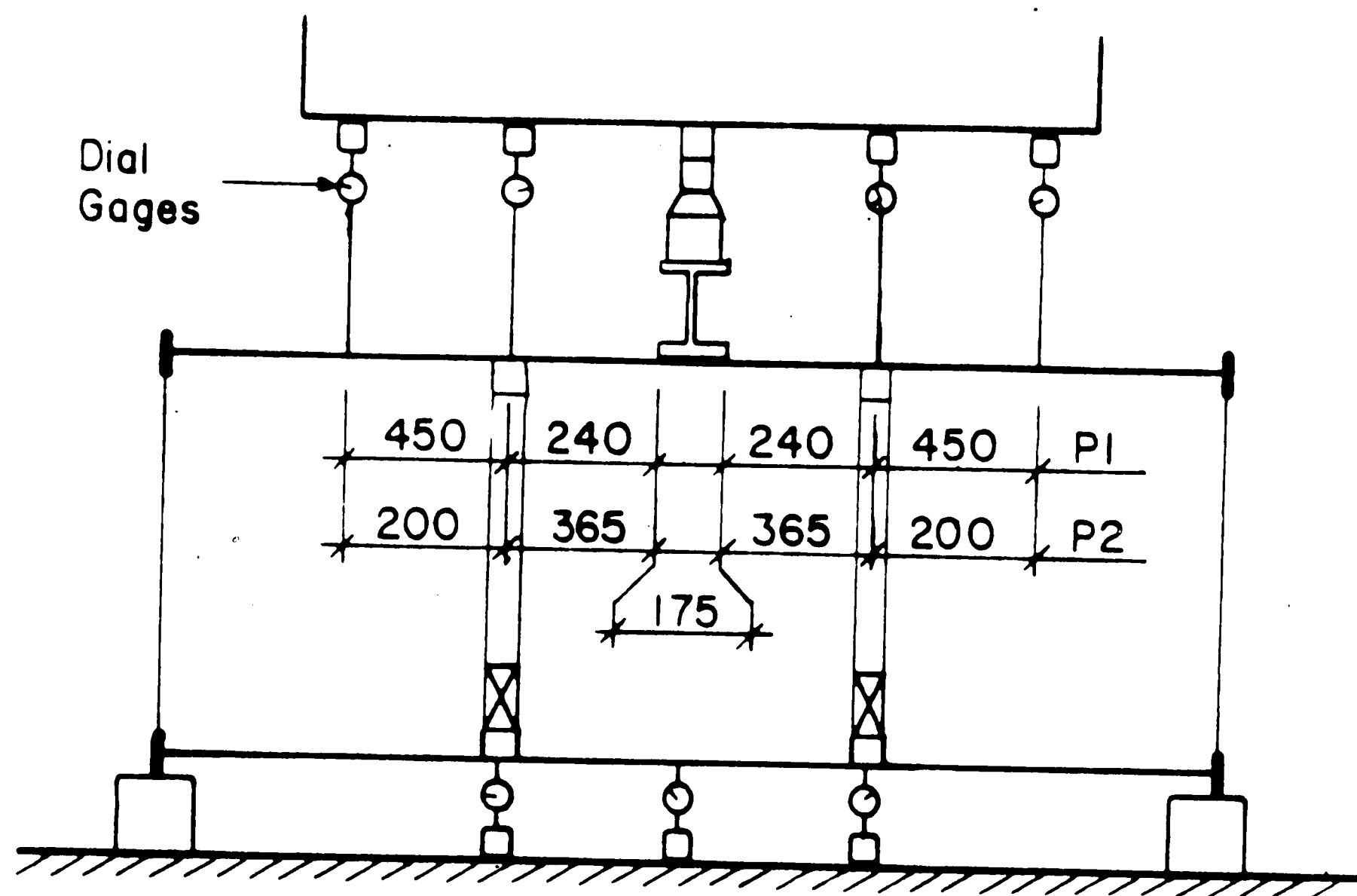
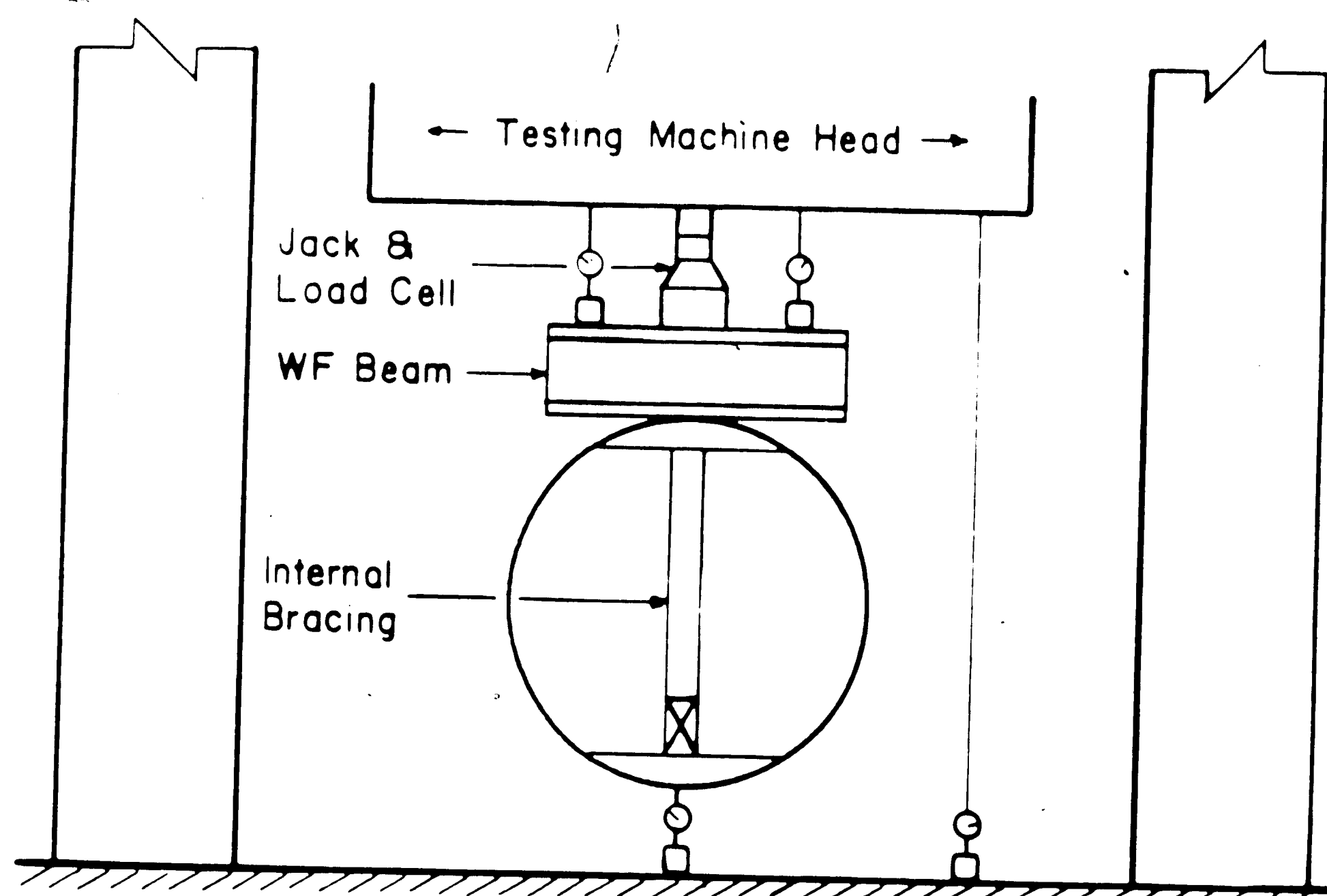


Figure 3: Schematic Representation of Ideal Dent Geometry



Dimensions in mm

Figure 4: Schematic Representation of Test Set-up for Indentation

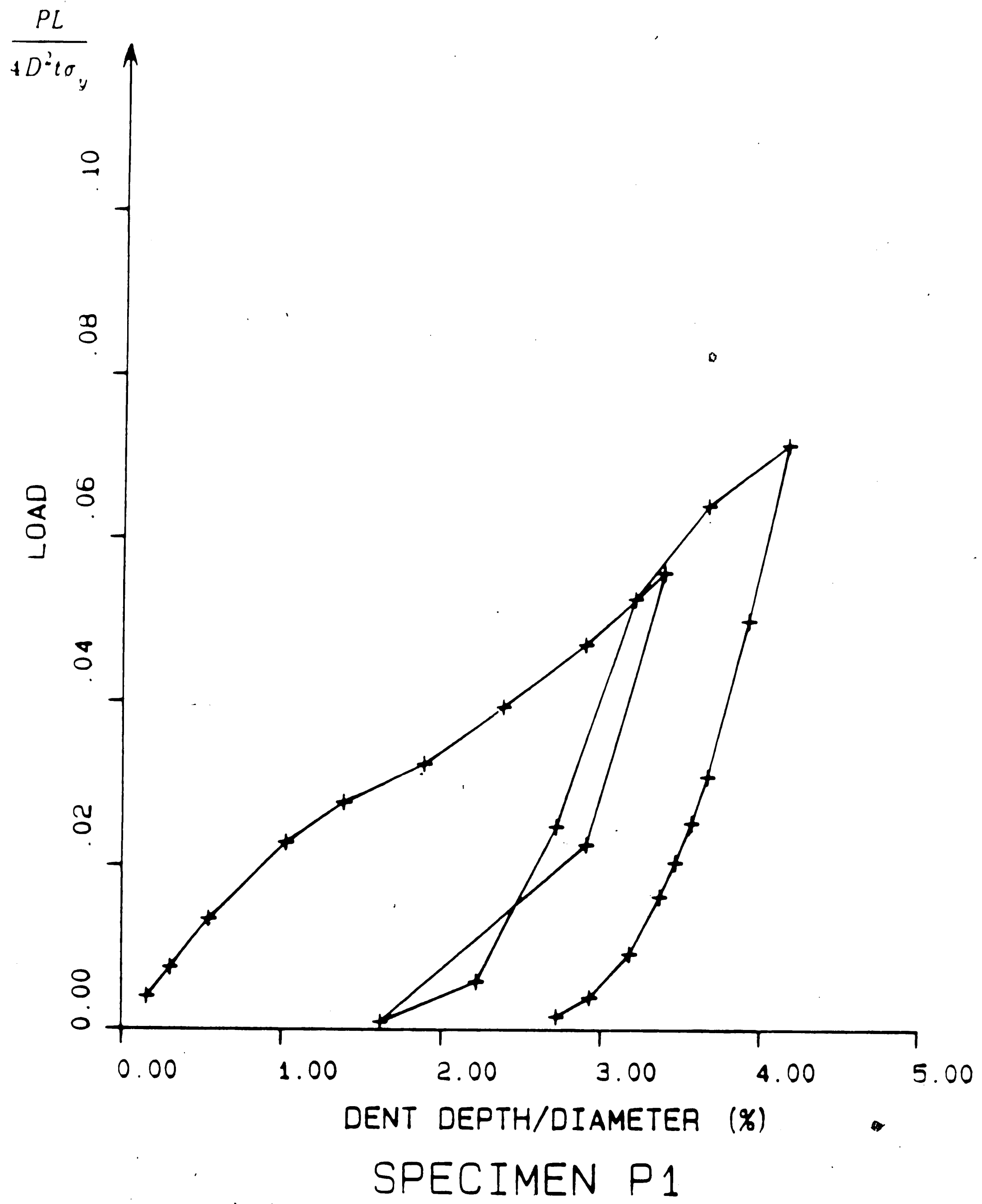


Figure 5: Experimental Load vs. Dent Depth Curve for Specimen P1

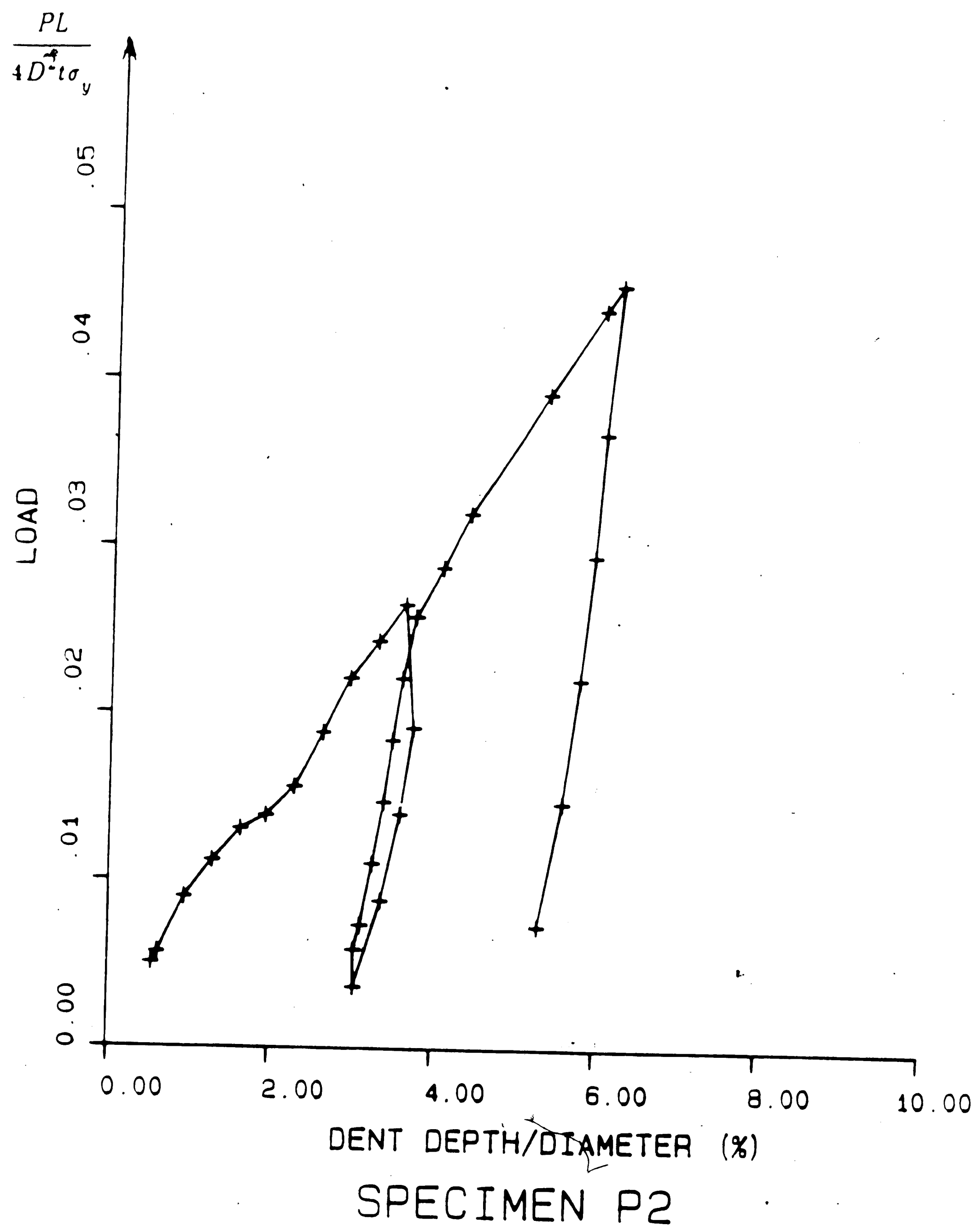


Figure 6: Experimental Load vs. Dent Depth Curve for Specimen P2

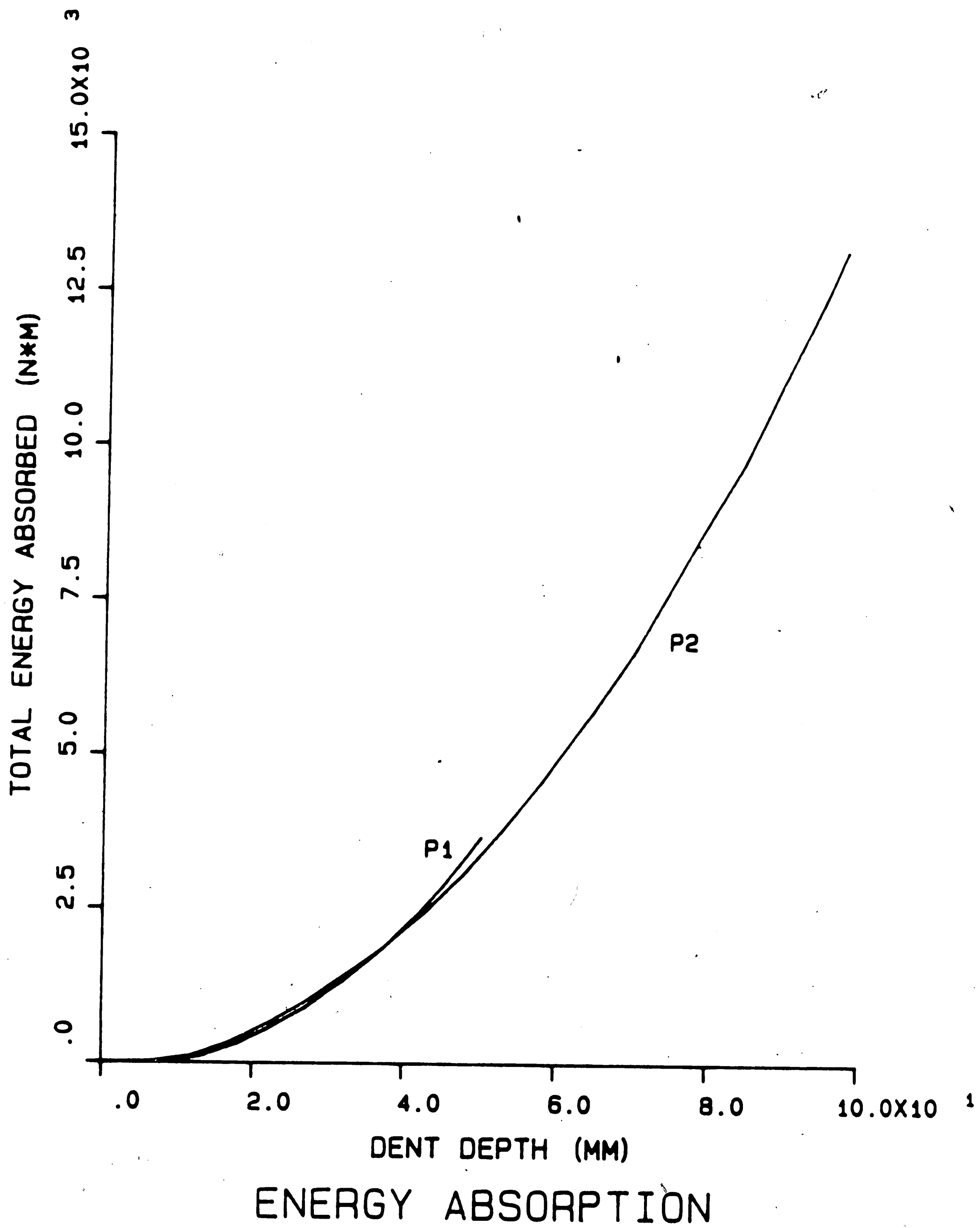


Figure 7: Energy Absorption vs. Dent Depth for Specimens P1 and P2

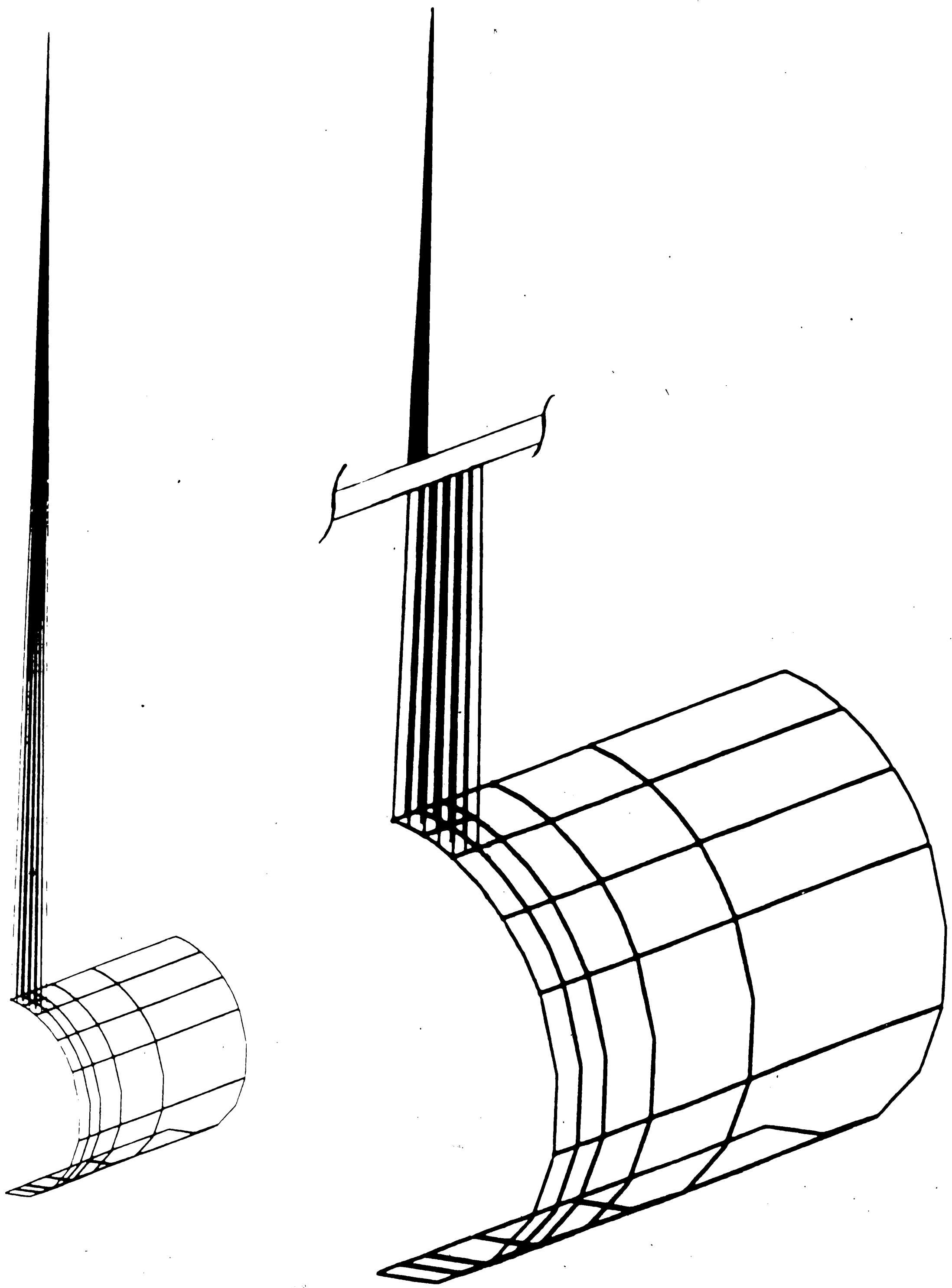


Figure 8: Finite Element Model for Tube Indentation

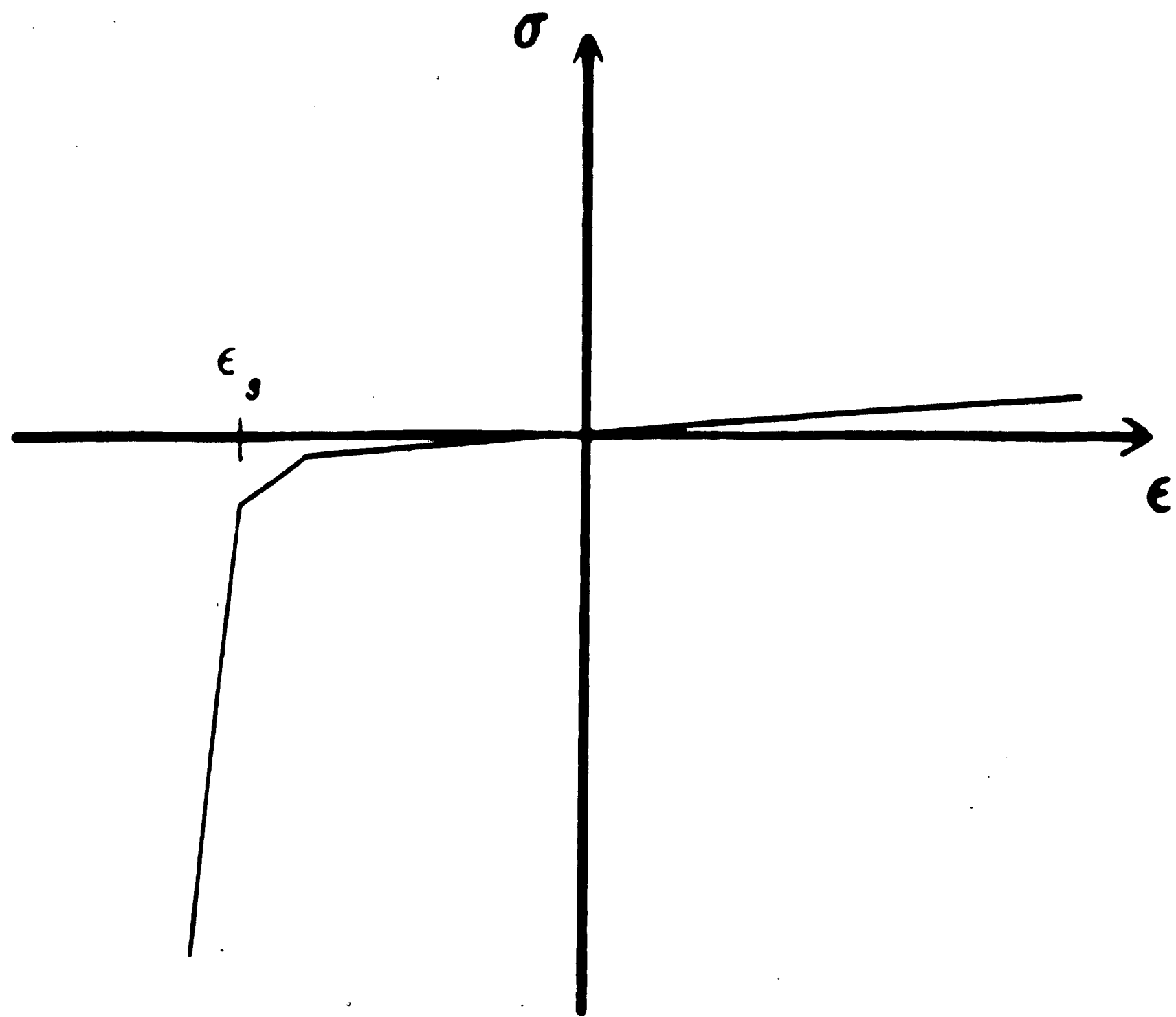


Figure 9: Typical Stress-Strain Relationship for Stiffening Truss Element

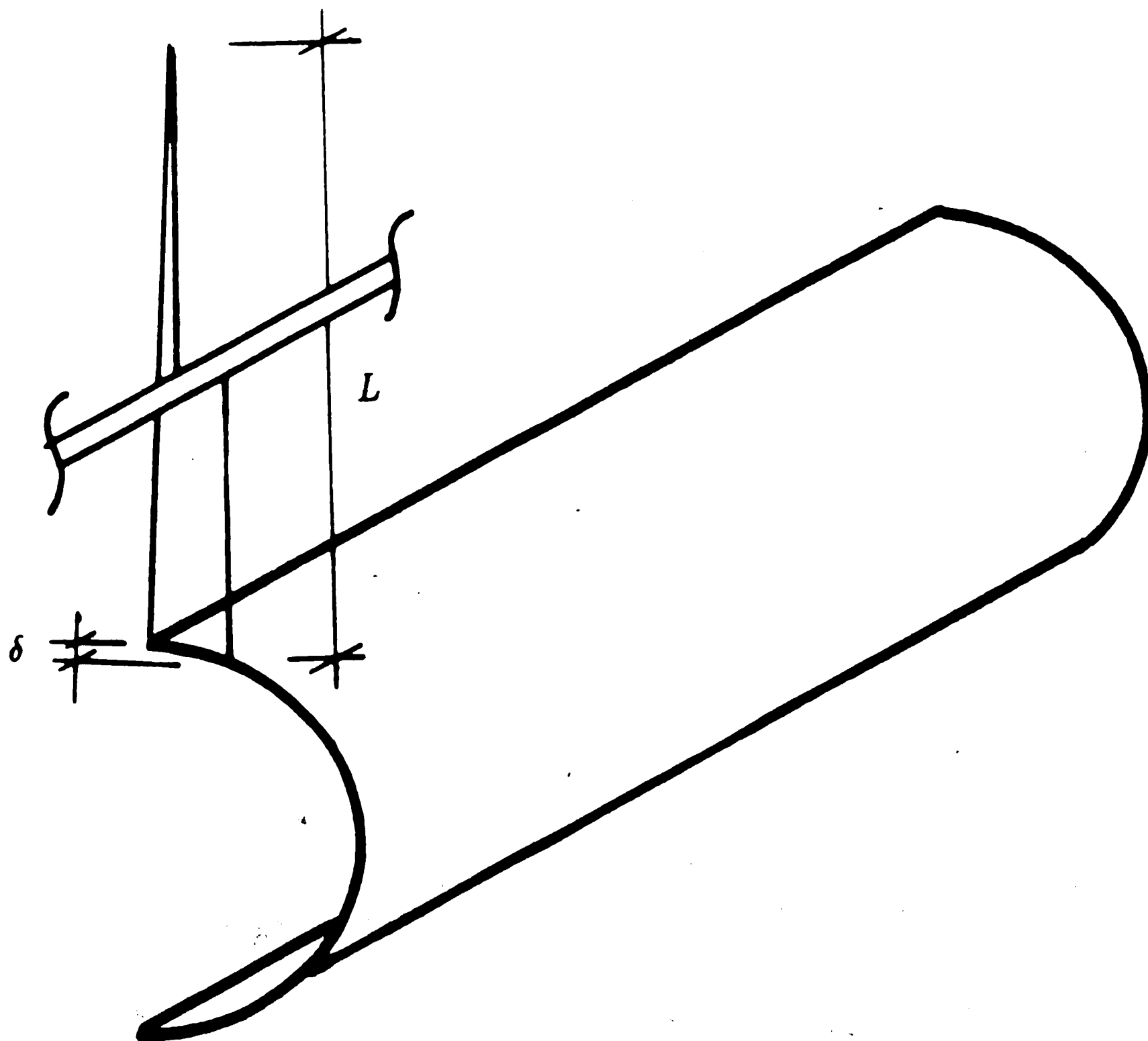


Figure 10: Geometry to Determine ϵ_g

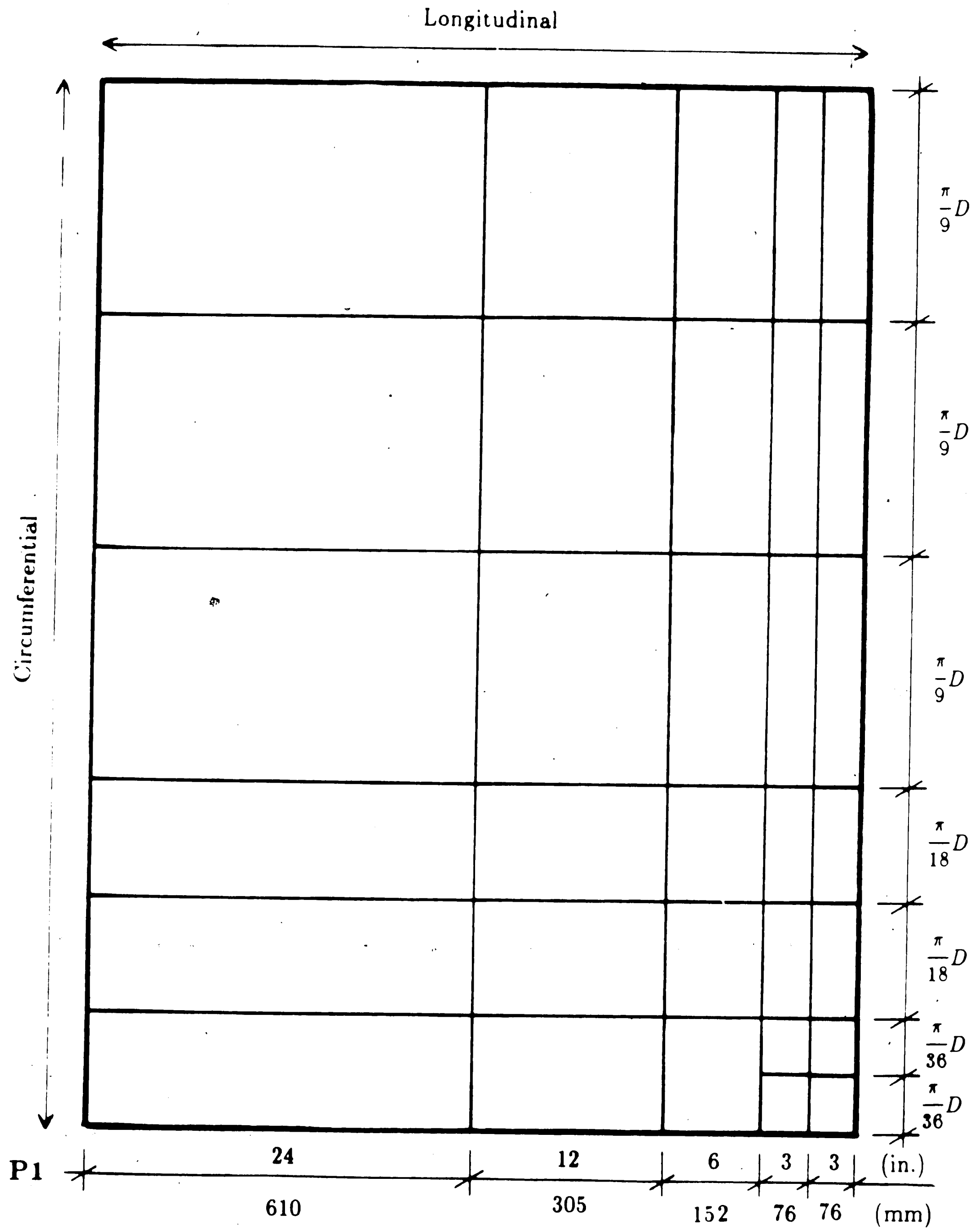


Figure 11: Dimensions for Discretization of Model 2

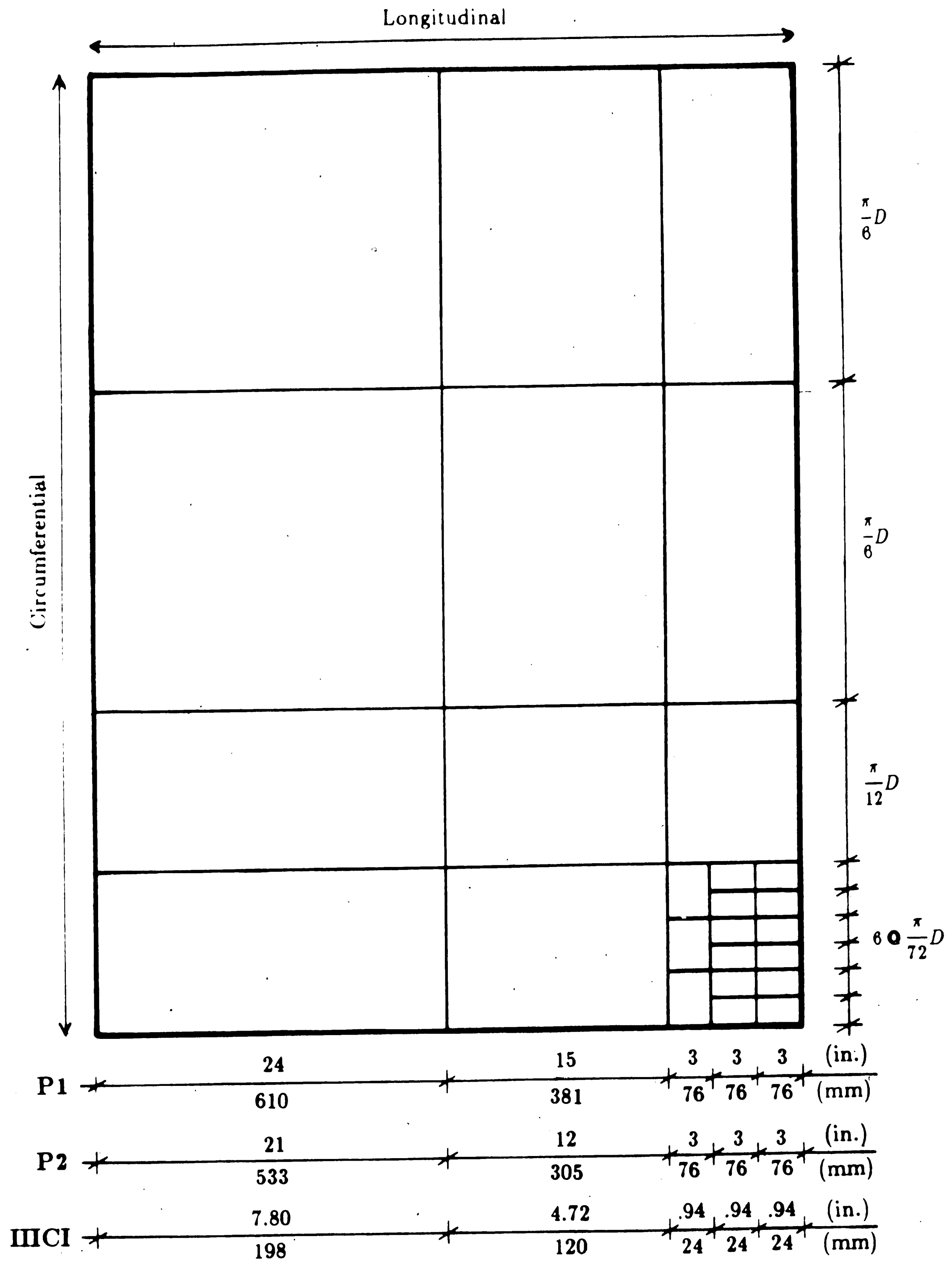


Figure 12: Dimensions for Discretization of Model 4

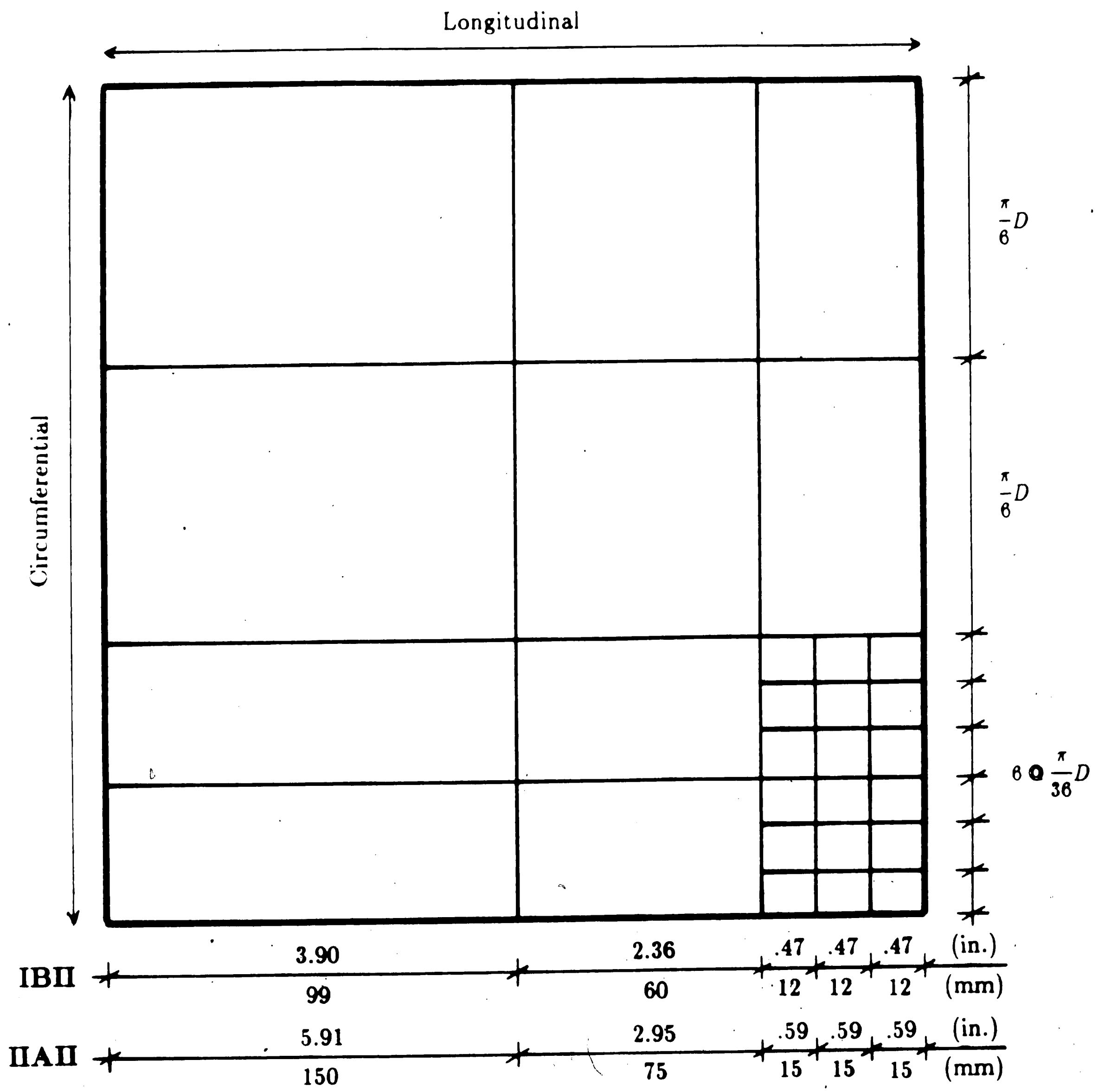


Figure 13: Dimensions for Discretization of Model 8

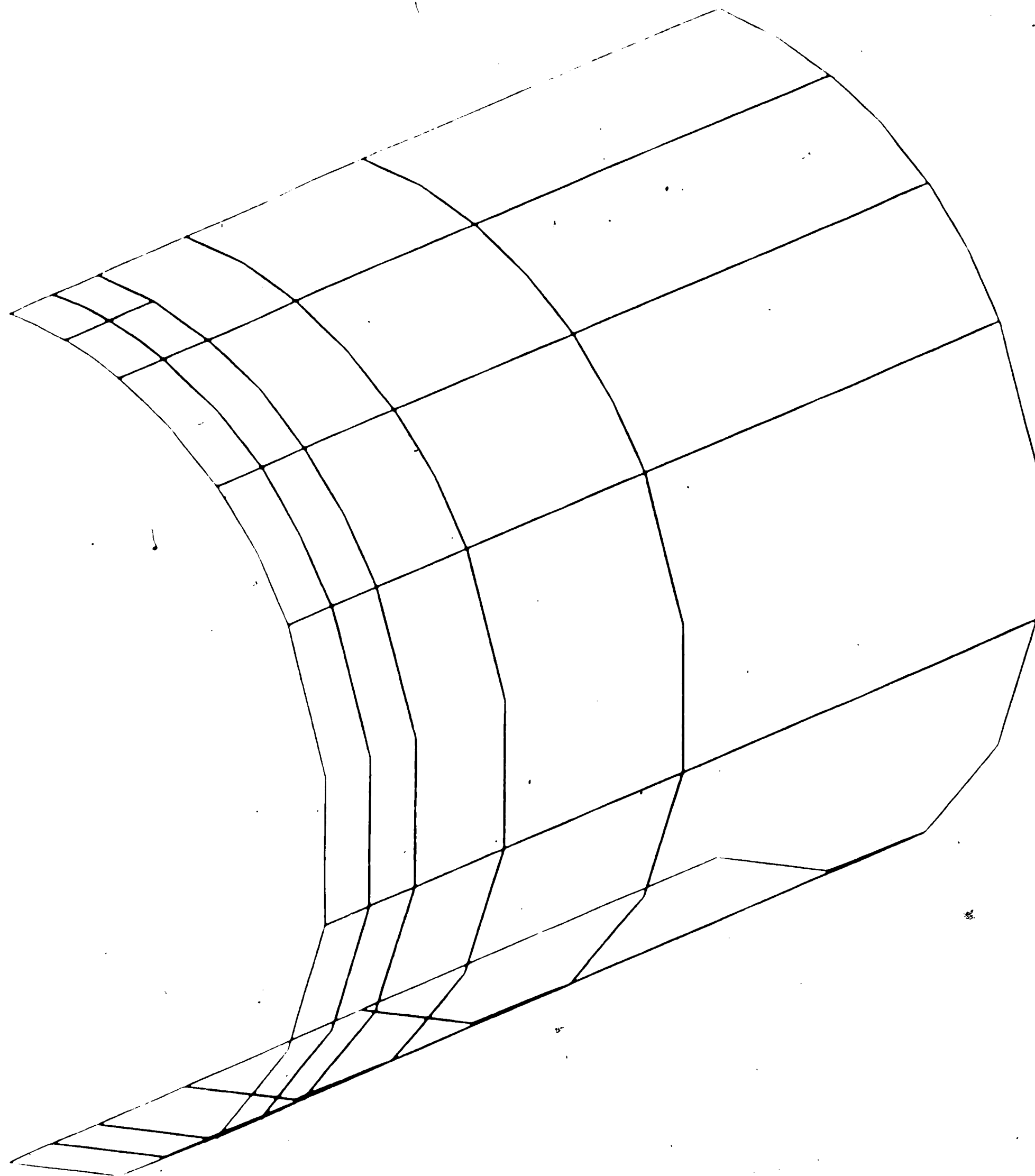


Figure 14: Discretization of Tube - Model 2

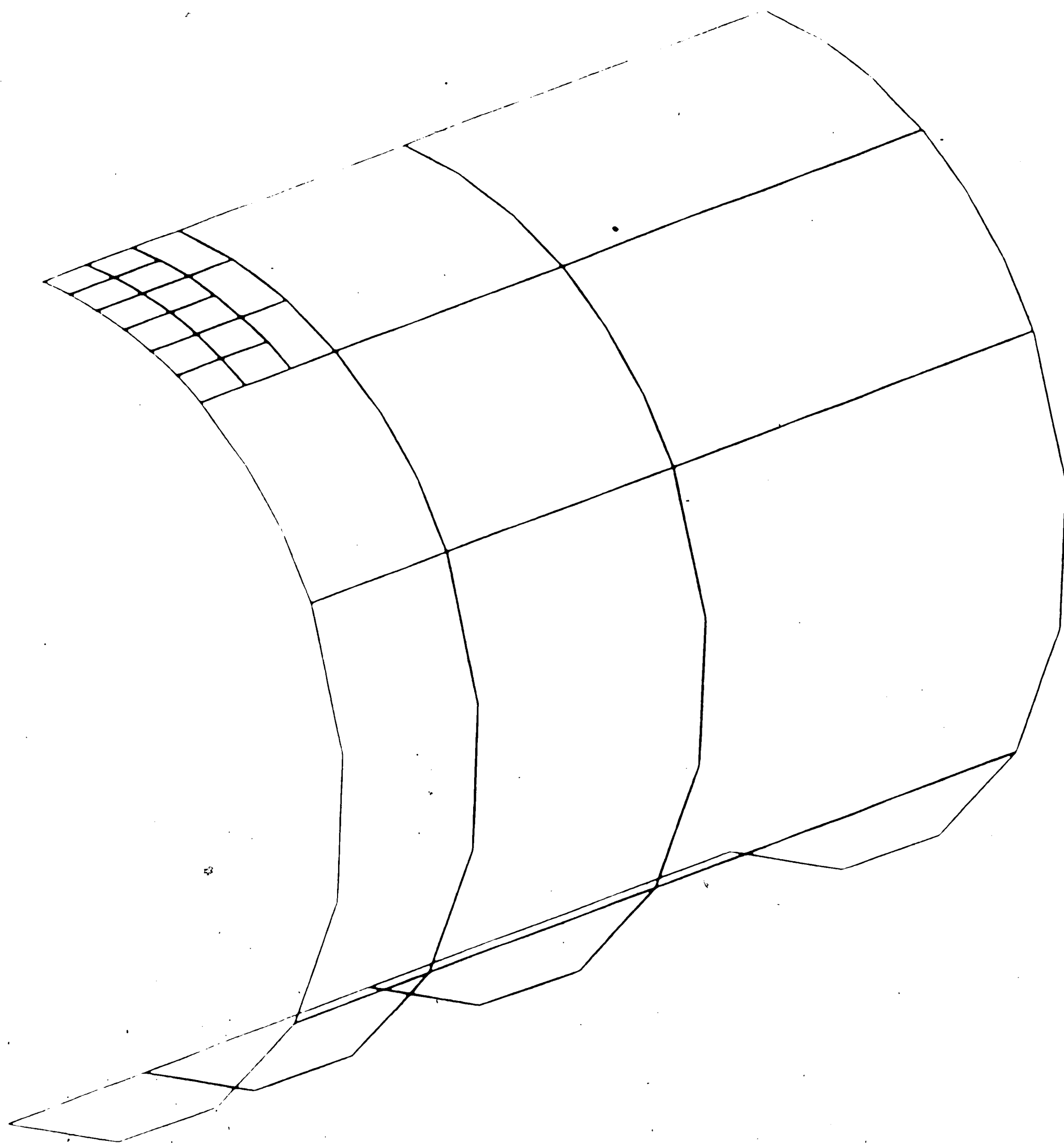


Figure 15: Discretization of Tube - Model 4

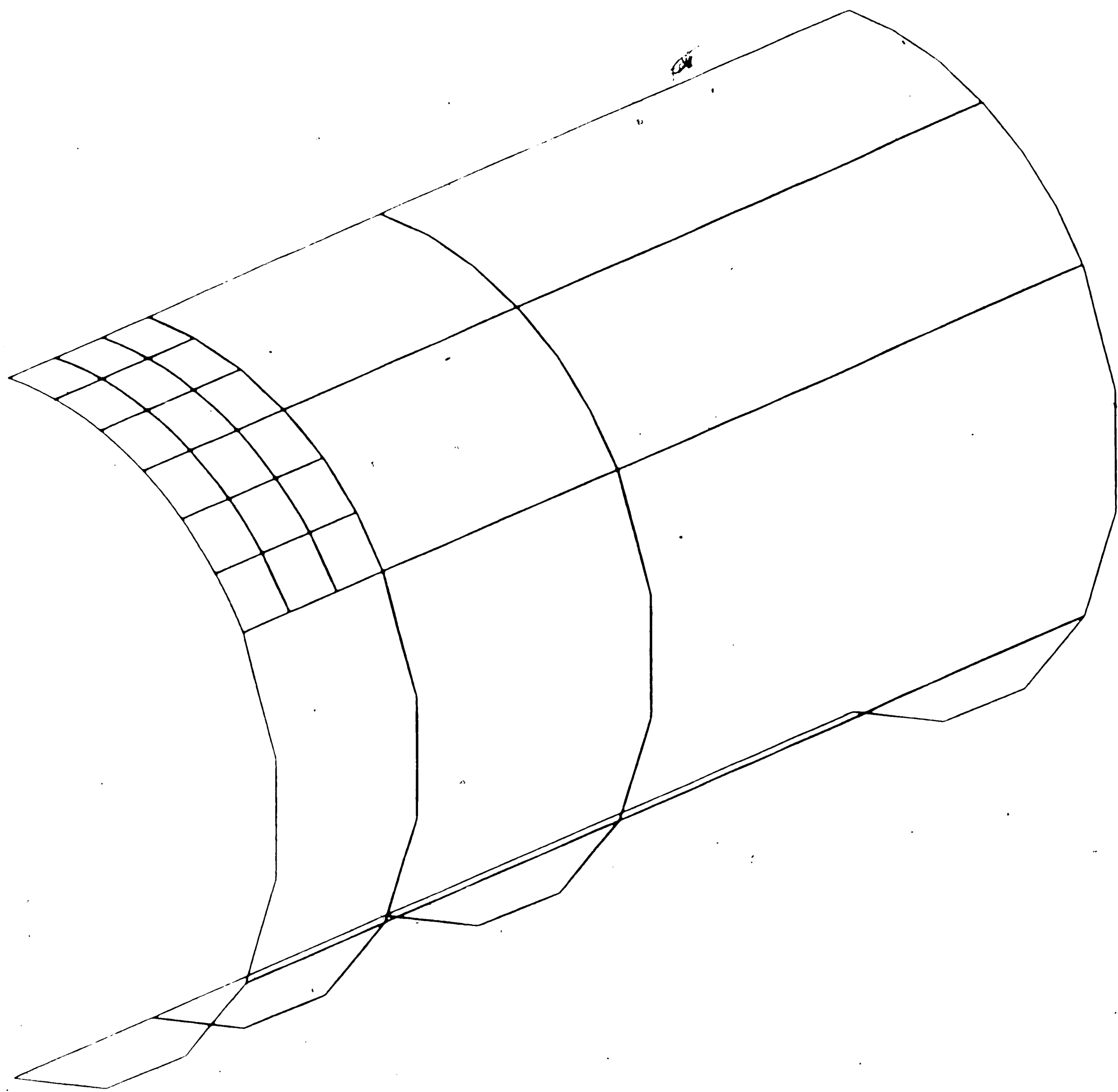
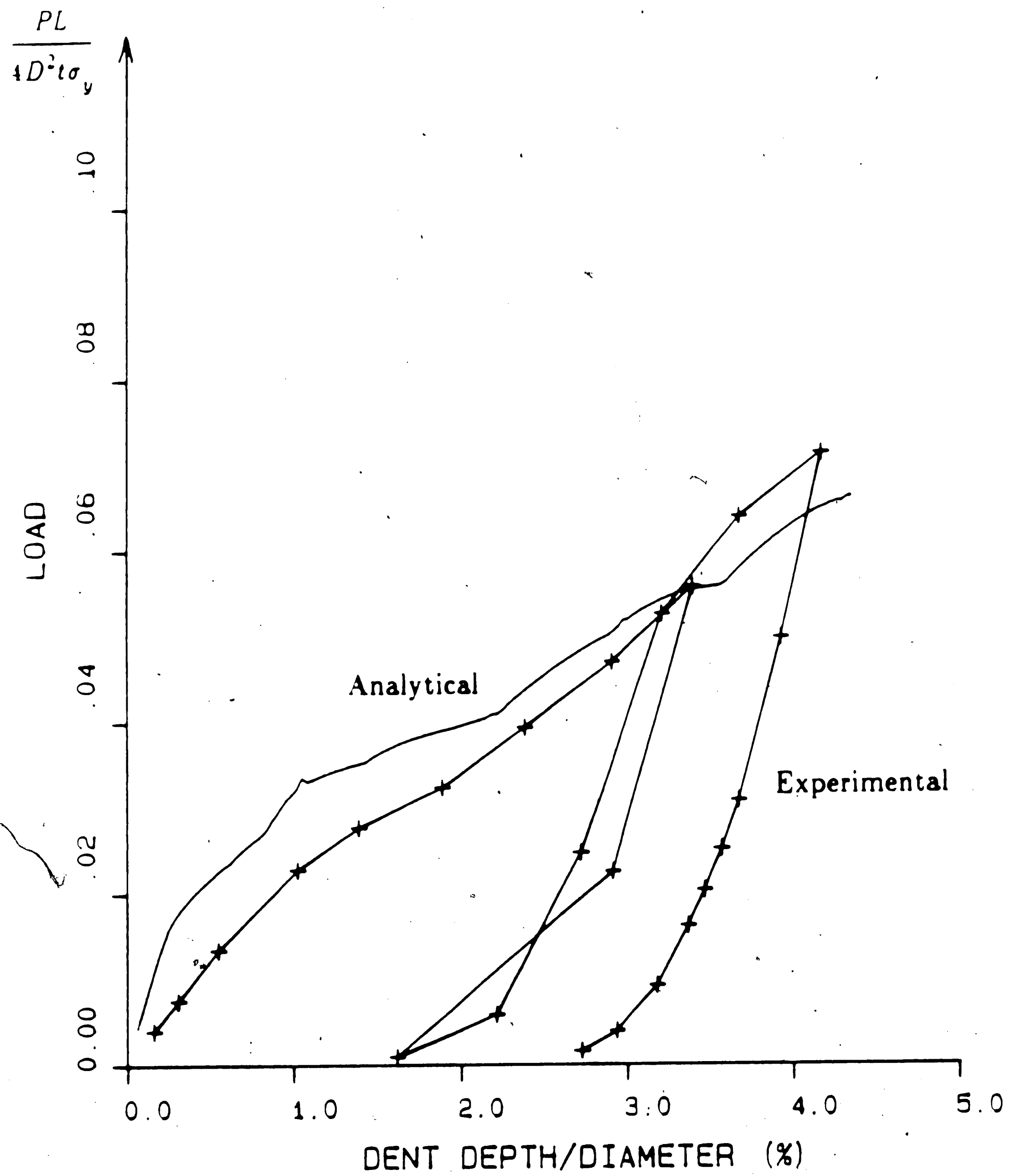


Figure 16: Discretization of Tube - Model 8



MODEL 2 - SPECIMEN P1

Figure 17: Load vs. Dent Depth, Speicmen P1 - Model 2

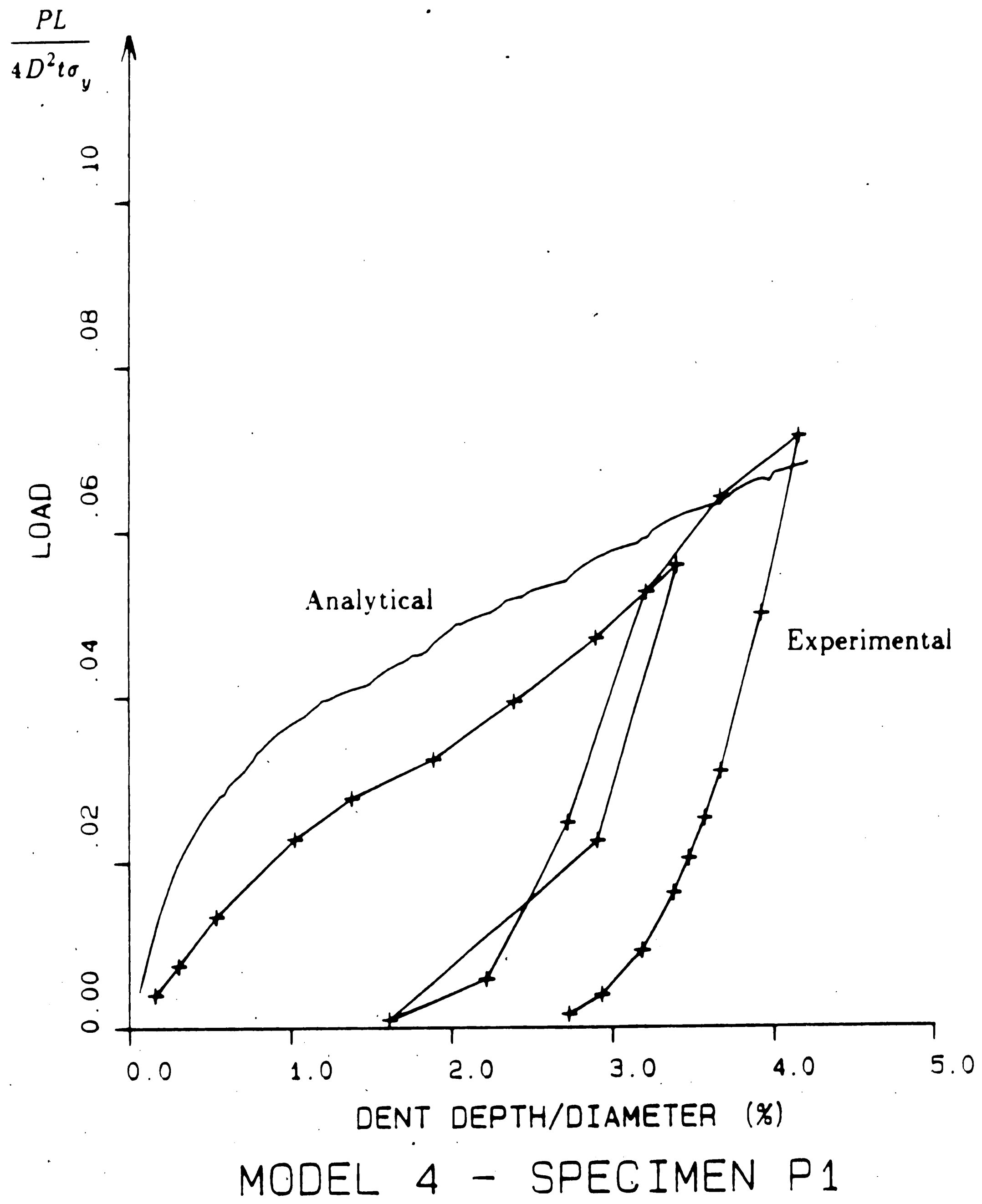


Figure 18: Load vs. Dent Depth, Specimen P1 - Model 4

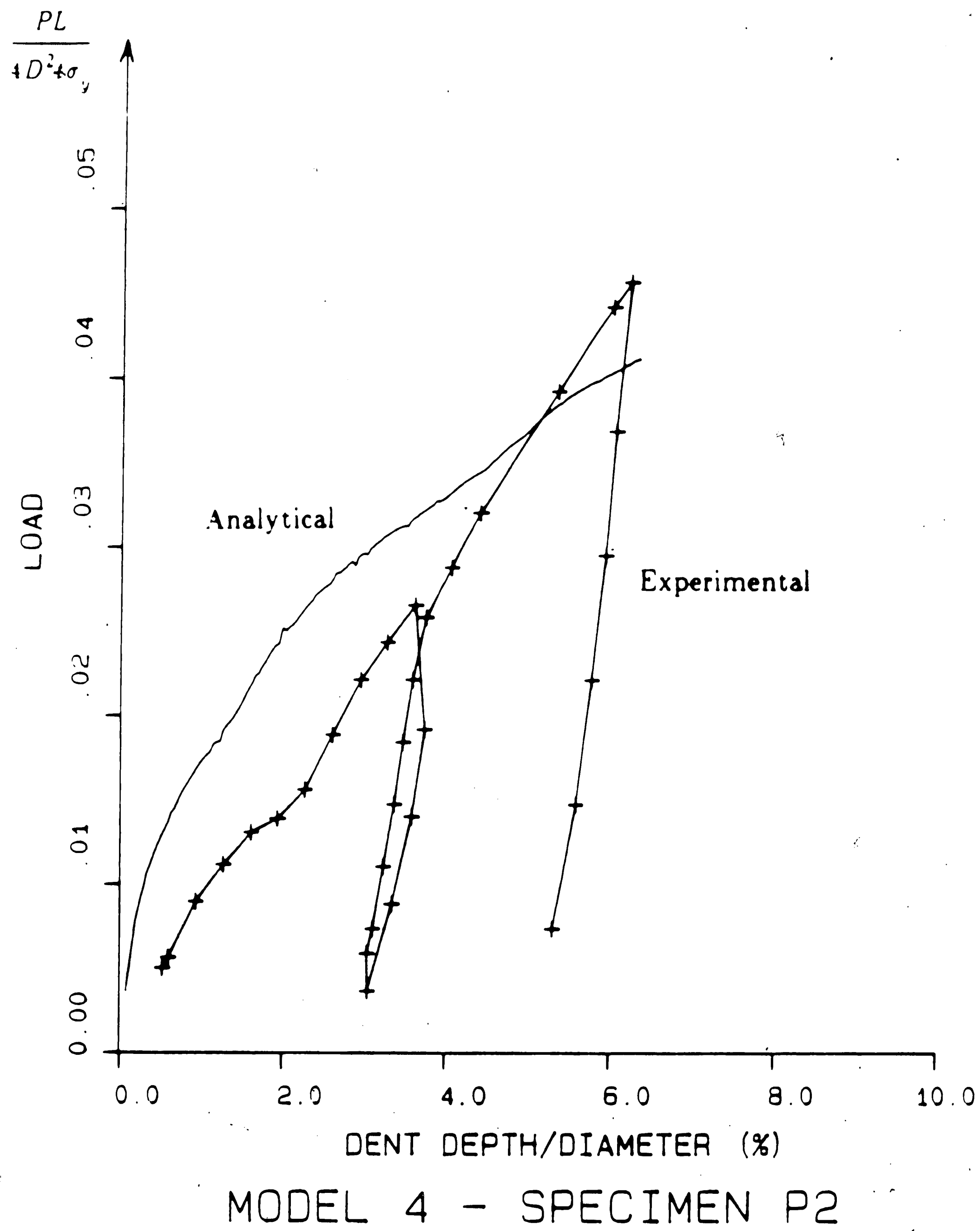


Figure 19: Load vs. Dent Depth, Specimen P2 - Model 4

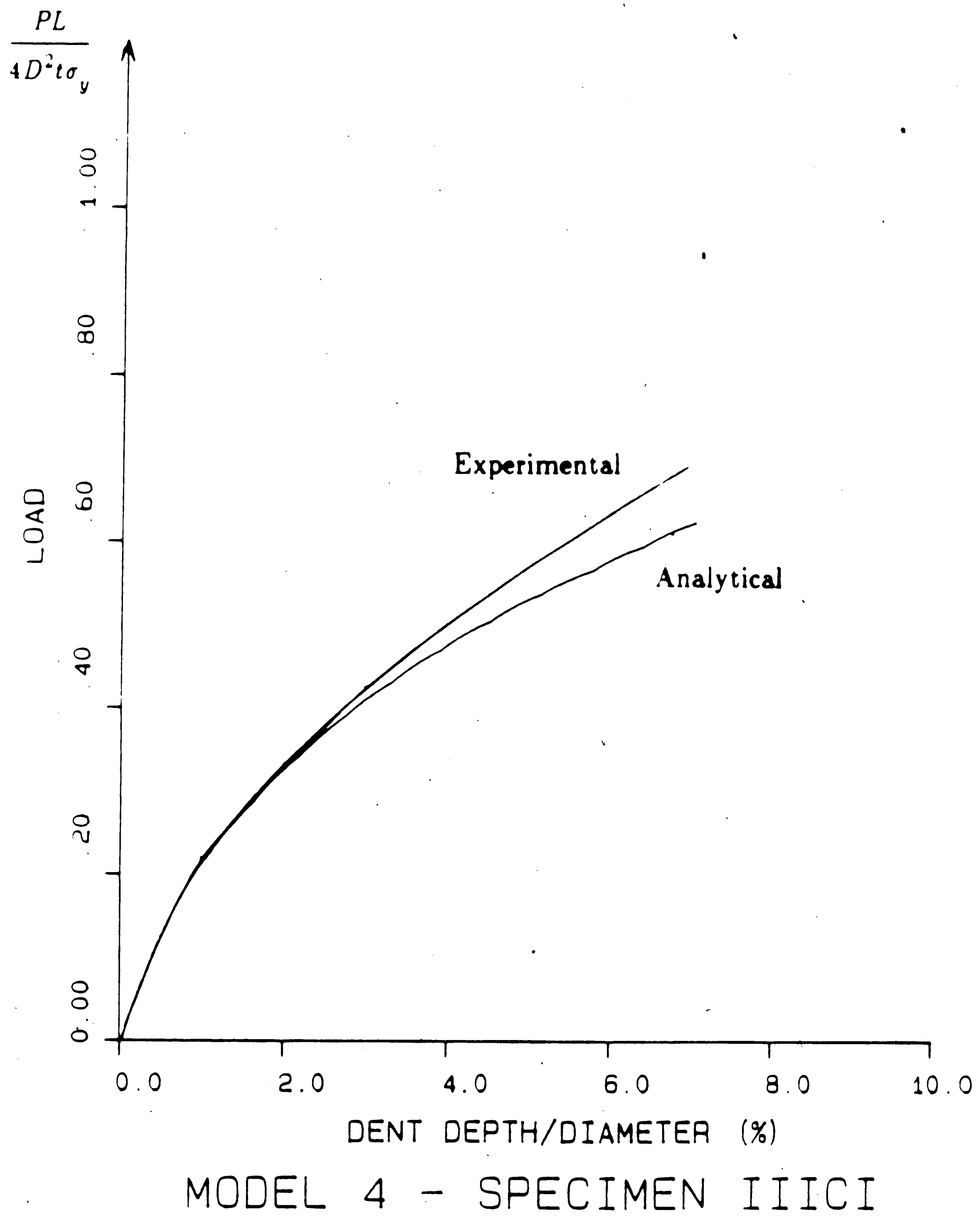
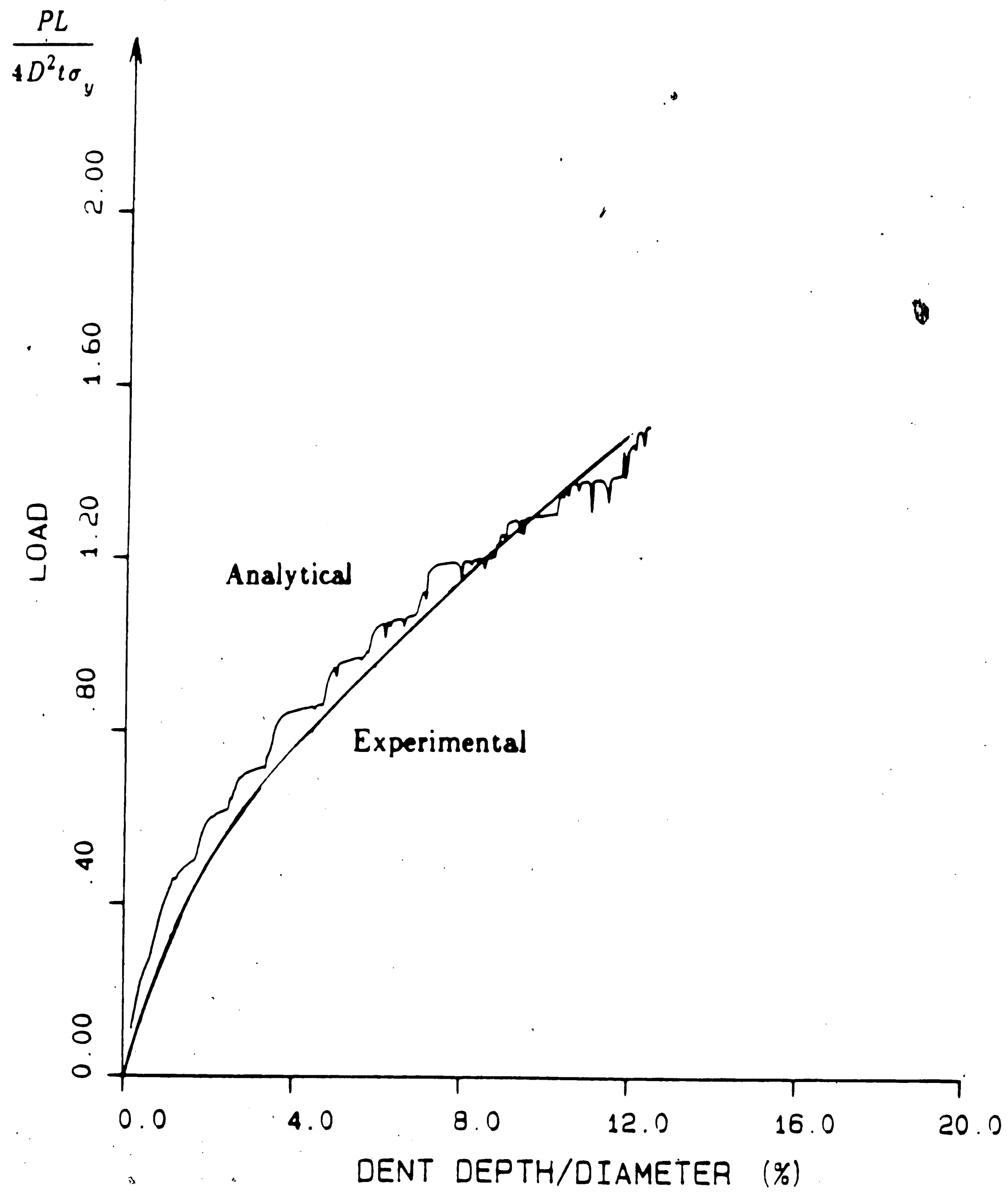
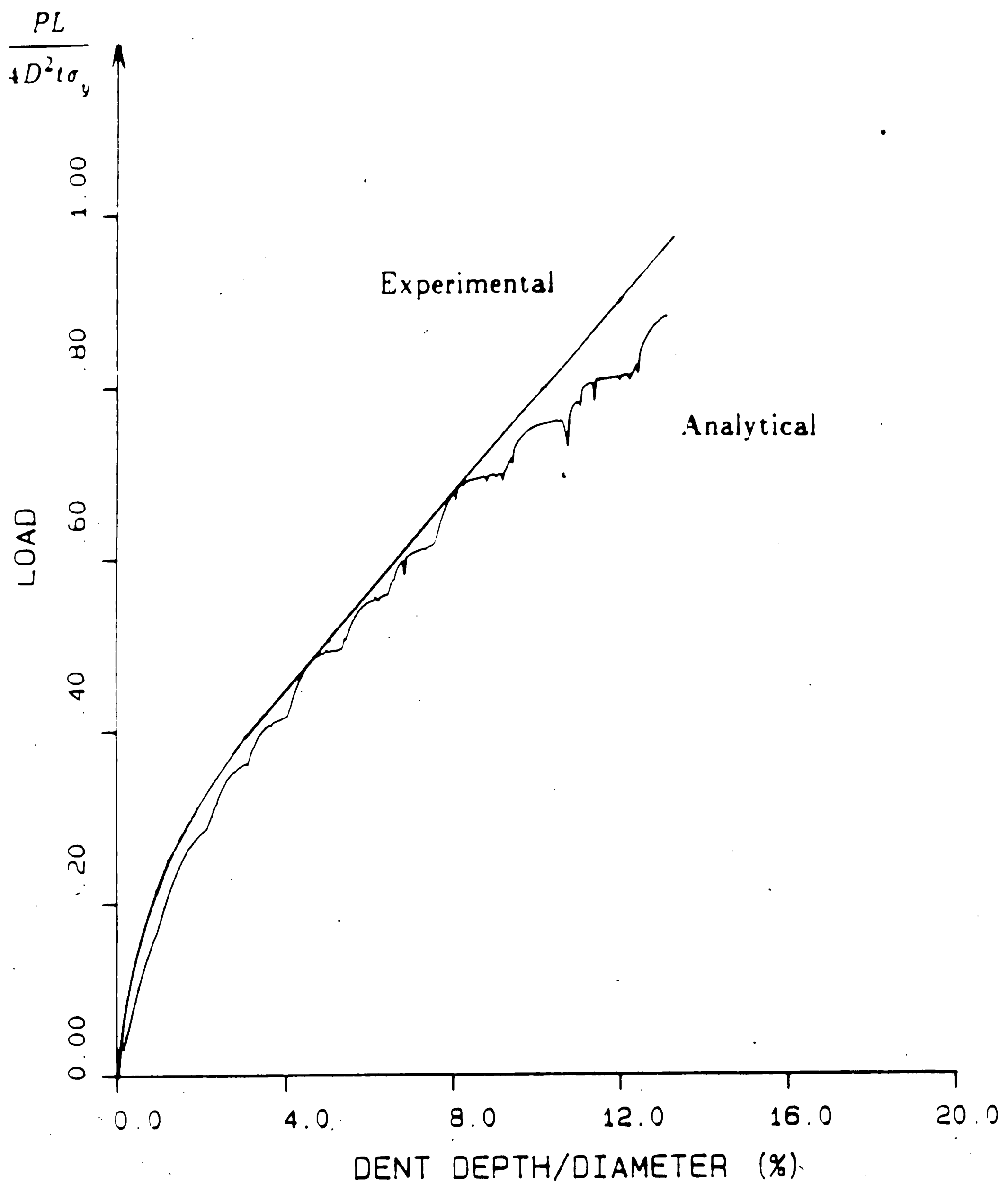


Figure 20: Load vs. Dent Depth, Speicmen IIICI - Model 4



MODEL 8 - SPECIMEN IBII

Figure 21: Load vs. Dent Depth, Specimen IBII - Model 8



MODEL 8 - SPECIMEN IIAII

Figure 22: Load vs. Dent Depth, Specimen IIAII - Model 8

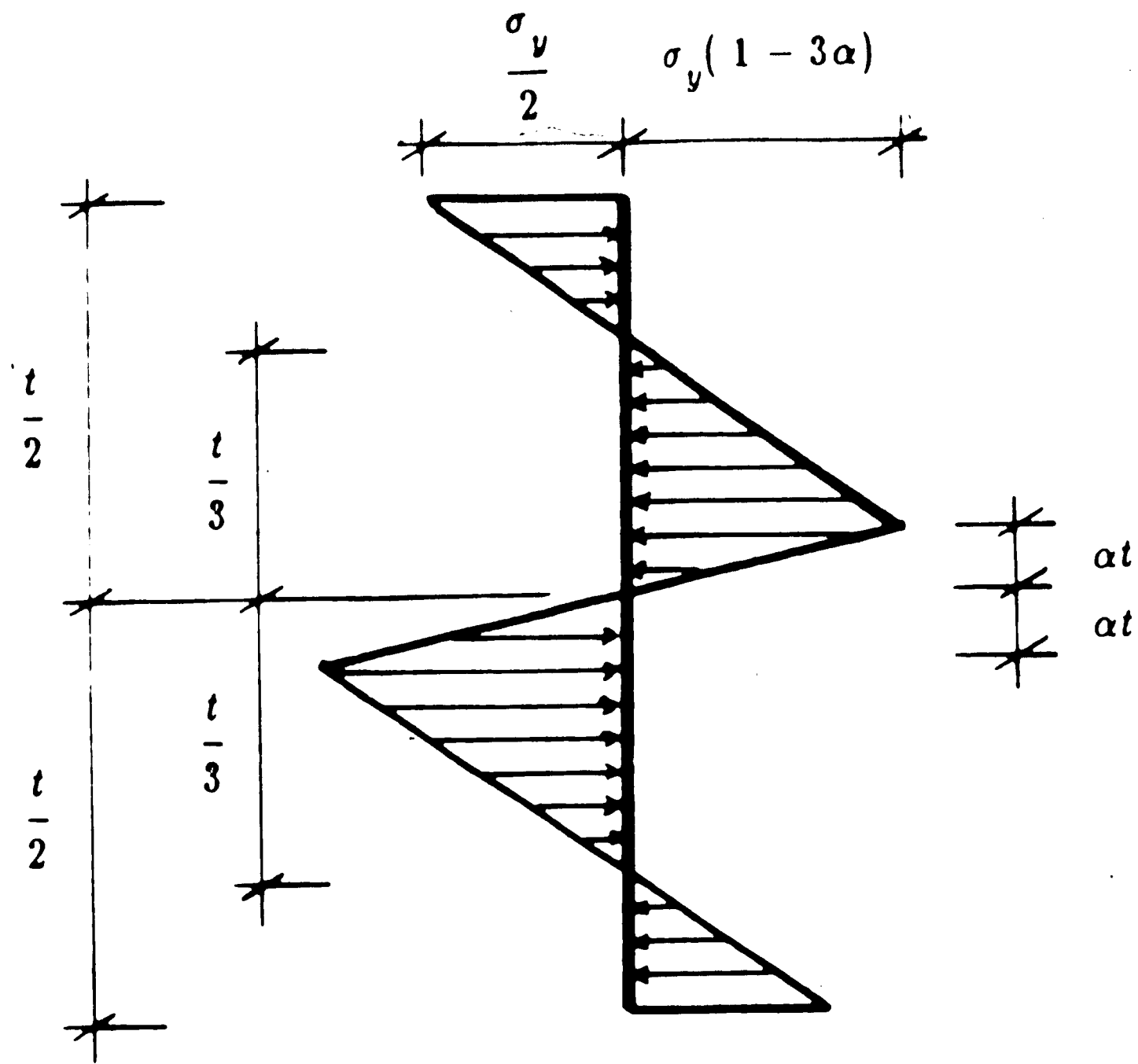


Figure 23: Residual Stresses Through Thickness Due to Cold-Rolling

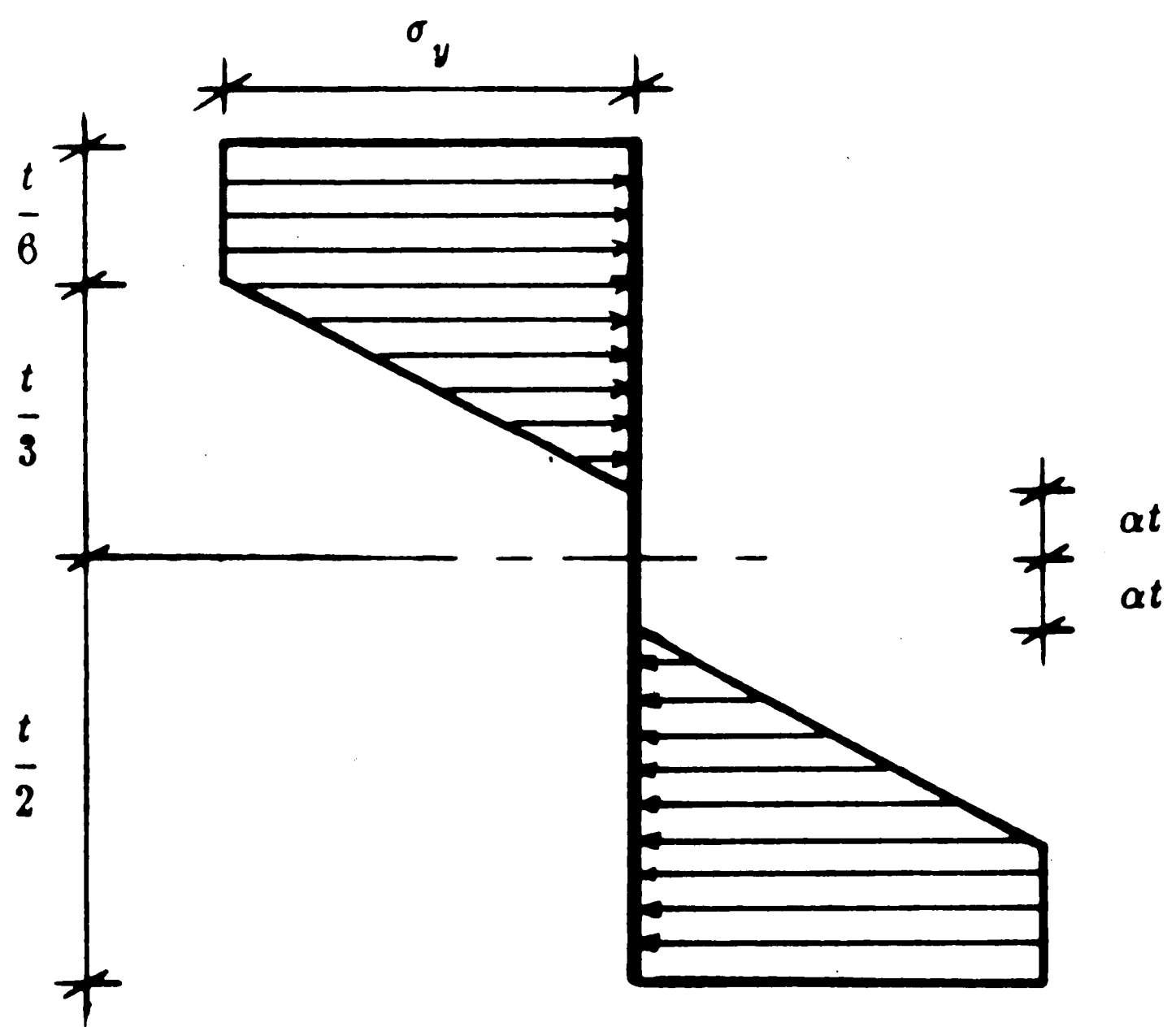


Figure 24: Stress Distribution after Flattening

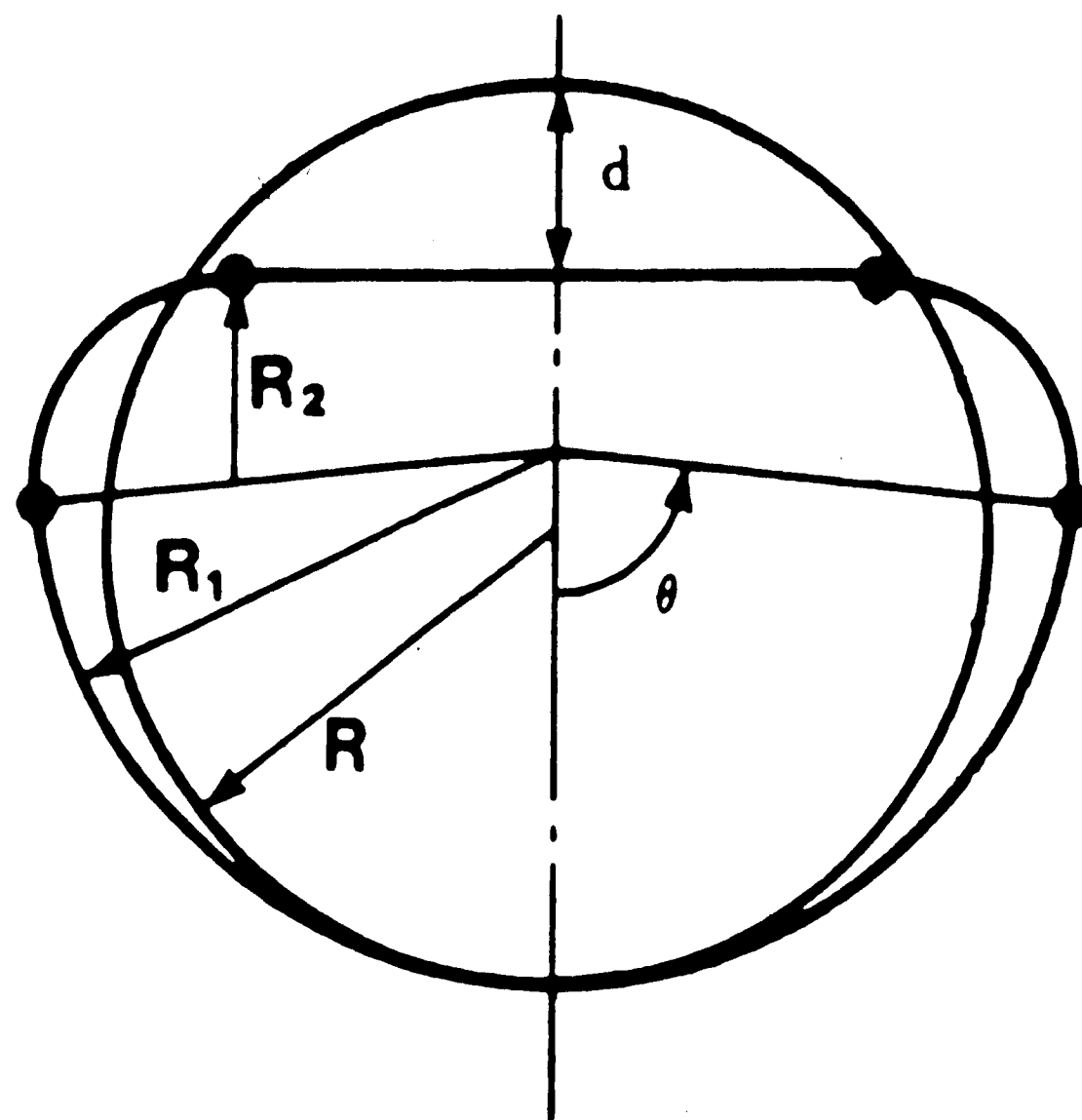


Figure 25: Assumed Deformation of a Ring
(From Reference [15])

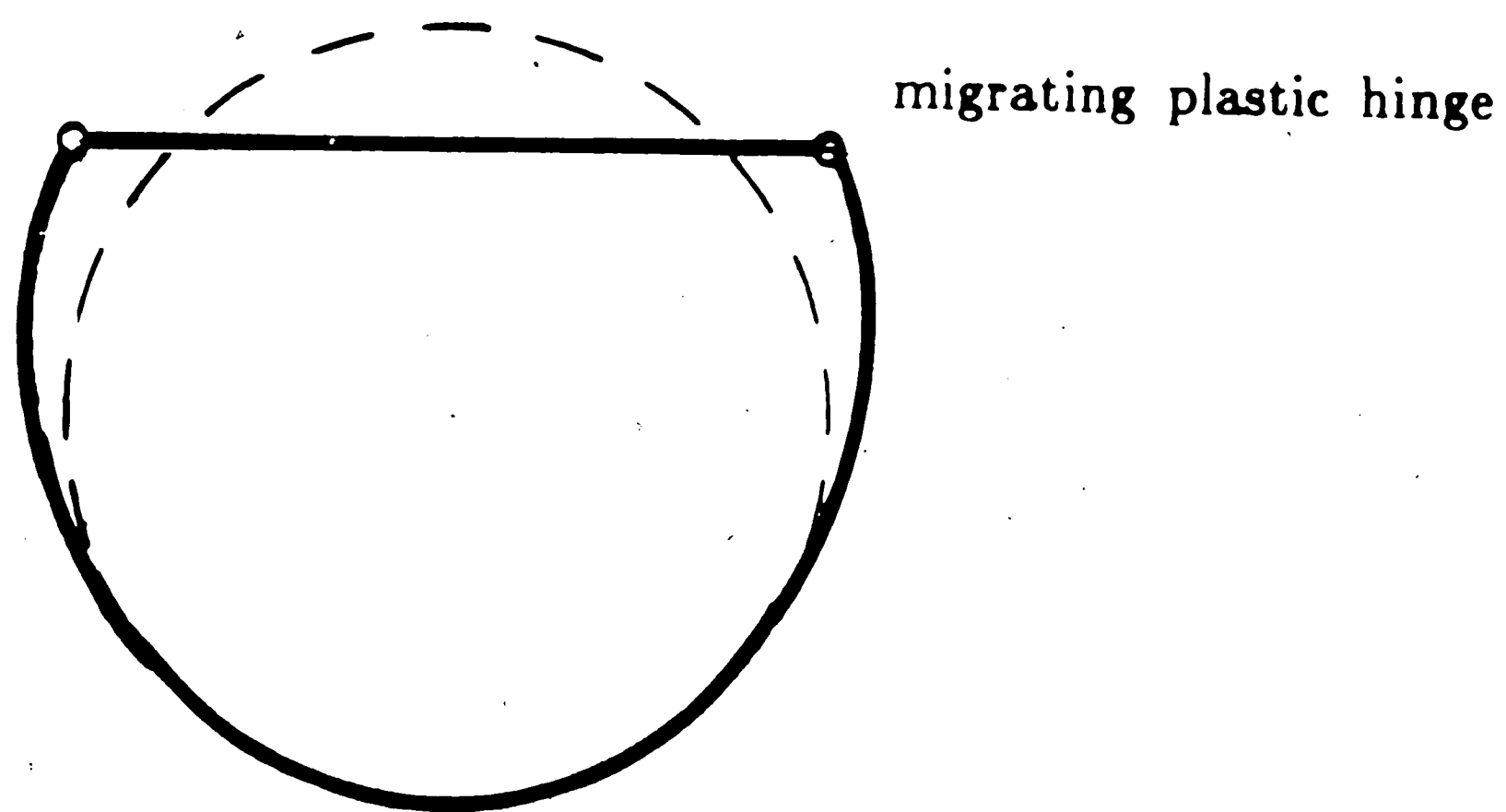


Figure 26: Deformation of a Ring from Idealized Dent Geometry

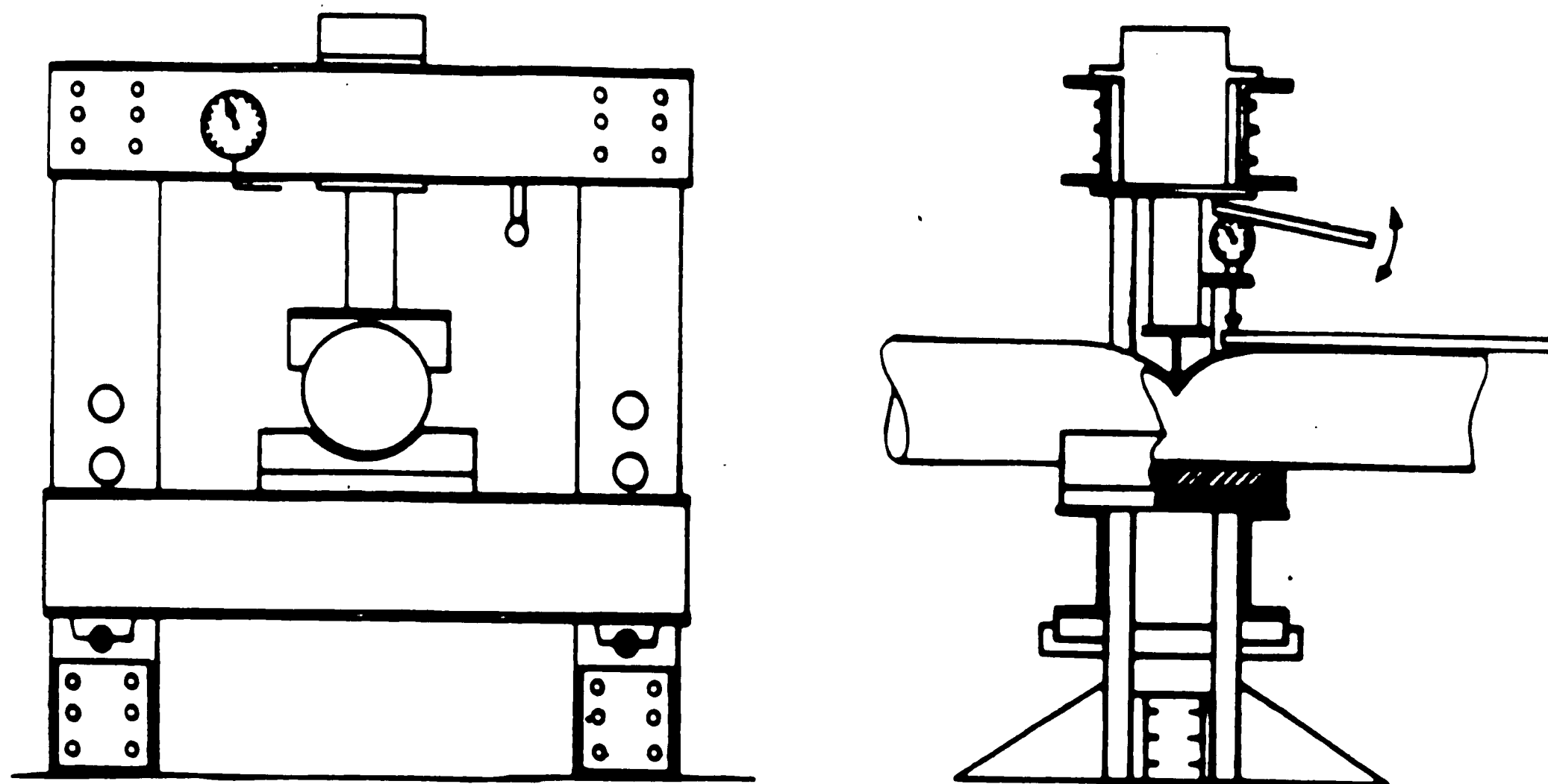


Figure 27: Test Setup for Indentation
(From Reference [12])

References

- [1] *ADINA User's Manual*
Report AE 81-1 edition, ADINA Engineering, Inc., 71 Elton Ave.,
Watertown, Mass. 02172, 1981.
- [2] *ADINA System Theory and Modeling Guide*
Report AE 83-4 edition, ADINA Engineering, Inc., 71 Elton Ave.,
Watertown, Mass. 02172, 1983.
- [3] Bathe, K.J.
Finite Element Procedures in Engineering Analysis.
Prentice-Hall, Inc., 1982.
- [4] Cook, R.D.
Concepts and Applications of Finite Element Analysis.
John Wiley & Sons, New York, 1981.
- [5] Ellinas, C.P., and Valsgard, S.
Collision and Damage of Offshore Structures: A State-of-the-Art.
In *Proceedings of the Fourth International Offshore Mechanics and Arctic
Engineering Symposium, Vol. 2*, pages 475-495. American Society of
Mechanical Engineers, New York, February, 1985.
(Symposium held in Dallas, TX, on February 17-21, 1985).
- [6] Grimm, D.F., and Ostapenko, A.
Local Buckling of Steel Tubular Columns.
In *Proceedings*, pages 25-28. Structural Stability Research Council,
Bethlehem, PA, 1982.
- [7] Hypponen, P. and Raiko, H.
Experiences in Nonlinear Shell Analysis Using Adina.
Computers and Structures 17(5-6):649-652, 1983.
- [8] Ostapenko, A., and Grimm, D.F.
Local Buckling of Cylindrical Tubular Columns Made of A-36 Steel.
Fritz Engineering Laboratory Report No. 450.7, Lehigh University,
Bethlehem, PA, February, 1980.
- [9] Padula, J.A., and Ostapenko, A.
Indentation and Axial Tests of Two Large-Diameter Tubular Columns.
Fritz Engineering Laboratory Report No. 508.5, Lehigh University,
Bethlehem, PA, February, 1987.
- [10] Sherman, D.R.
Tests of Circular Steel Tubes in Bending.
Journal of the Structural Division, ASCE 102(ST11, Paper
12568):2181-2195, November, 1976.

- [11] Soares, C.G., and Soreide, T.H.
Plastic Analysis of Laterally Loaded Circular Tubes.
Journal of Structural Engineering, ASCE 109(2):451-467, February, 1983.
- [12] Taby, J., and Rashed, S.M.H.
Experimental Investigation of the Behaviour of Damaged Tubular Members.
Technical Report MK/R92, Department of Naval Architecture and Marine
Engineering, The Norwegian Institute of Technology, Trondheim,
Norway, 1980.
- [13] Taby, J., and Moan, T.
Collapse and Residual Strength of Damaged Tubular Members.
Behaviour of Offshore Structures.
Elsevier Science Publishers B.V., Amsterdam, 1985, pages 395-408.
- [14] Thomas, S.G., Reid, S.R., and Johnson, W.
Large Deformations of Thin-Walled Circular Tubes under Transverse
Loading-I.
International Journal of Mechanical Sciences 18(6):325-333, June, 1976.
- [15] Wierzbicki, T., and Suh, M.S.
Denting Analysis of Tubes Under Combined Loading.
Technical Report MITSG 86-5, MIT Sea Grant College Program,
Massachusetts Institute of Technology, 77 Massachusetts Ave.,
Cambridge, MA 02139, March, 1986.
NA84AA-D-0046 R/O-19.
- [16] Wierzbicki, T., and Bhat, S.U.
A Moving Hinge Solution for Axisymmetric Crushing of Tubes.
International Journal of Mechanical Sciences 28(3):135-151, 1986.

Appendix A

Experimental Work by Others

Experimental data reported by other researchers was used to assess the validity of the finite element analysis. Specifically, the indentation behavior of three specimens selected from Reference [12] (Specimens IIII, IBII, and IIAI) was analyzed and the results compared to the experimental data. The experimental work on these three specimens is described here since the details are relevant to understanding the conclusions drawn from the analytical work.

A.1 Scope

The experimental work described in Reference [12] was part of a study to form the basis of a simplified analytical method for determining the residual strength of dented tubular columns. This work included indentation and axial load tests of 24 tubular members. Experimental load vs. dent depth curves were presented for the 24 specimens as well as a comparison of the theoretical and experimental axial strengths of the dented specimens.

A.2 Description of Test Specimens

The test specimens were cold-drawn manufactured seamless tubes which were heat treated to relieve residual stresses from the manufacturing process and improve ductility.** The heat treatment consisted of heating to 550°C (1020°F) for one hour followed by slow cooling.

The specimen geometries were representative of a 1:4 scaling of members

** Pertinent information, including geometric data and material properties of the three specimens analyzed, is listed in Table 1.

commonly found in offshore structures. The D/t ratios of the specimens varied from 40 to 64 with diameters ranging from 125 to 250 mm (5 to 10 in.). All specimens had a length of 3500 mm (138 in.). The dent depth of the specimens ranged from 2% to 20% of the diameter.

A.3 Indentation of Specimens

The method of indentation of the specimens was different from that used for Specimens P1 and P2. The objective of the indentation process was to produce specimens without overall bending deformations so that the effect of indentations could be isolated. To accomplish this, the tubes were supported in a wooden cradle directly below the indenter as shown in Fig. 27. The denting force was transmitted to the tube through a "knife edge" (5 mm radius) indenter. During indentation, the dent depth and the load, provided by a hydraulic jack, were measured with a dial gage and manometer, respectively. Although not indicated on the load vs. dent depth curves presented in the reference, the specimens required multiple load cycles to produce the desired dent depths.

The type of support and the "knife edge" loading were the principal considerations in modeling these specimens for the finite element analysis.

Appendix B

Nomenclature

D	Diameter
d	Dent depth
L	Length
R	Radius
R_1, R_2	Radii as defined in Fig. 25
r_2	Nondimensionalized Radius = $\frac{R_2}{R}$
t	Thickness
α	Coefficient = $\frac{D \epsilon_y}{2t} + 3 \epsilon_y$
δ	Gap Distance between indenter and tube wall
ϵ	Strain (engineering)
ϵ_y	Yield Strain
Φ	Curvature
Φ_y	Yield Curvature = $\frac{2\epsilon_y}{t}$
σ	Stress
σ_y	Yield Stress
θ	Angle as defined in Fig. 25

Vita

Joseph A. Padula is the son of Helen and Joseph A. Padula and was born on March 8, 1955 in San Diego, California.

He graduated from Lake Taylor Senior High School in Norfolk, Virginia in 1971. His undergraduate studies were taken at Virginia Polytechnic Institute and State University, Blacksburg, Virginia and at Old Dominion University in Norfolk, Virginia. In 1985, he was awarded the Bachelor of Science in Civil Engineering from Old Dominion University. Graduate studies were undertaken in the fall of 1985 in the Department of Civil Engineering at Lehigh University where he has been a teaching and research assistant.